



**HAL**  
open science

# Monte Carlo Simulation for the Spin Transport in Magnetic Thin Films

K. Akabli, H. T. Diep

► **To cite this version:**

K. Akabli, H. T. Diep. Monte Carlo Simulation for the Spin Transport in Magnetic Thin Films. 2008.  
hal-00318711

**HAL Id: hal-00318711**

**<https://hal.science/hal-00318711>**

Preprint submitted on 4 Sep 2008

**HAL** is a multi-disciplinary open access archive for the deposit and dissemination of scientific research documents, whether they are published or not. The documents may come from teaching and research institutions in France or abroad, or from public or private research centers.

L'archive ouverte pluridisciplinaire **HAL**, est destinée au dépôt et à la diffusion de documents scientifiques de niveau recherche, publiés ou non, émanant des établissements d'enseignement et de recherche français ou étrangers, des laboratoires publics ou privés.

## CHAPTER 1

### Monte Carlo Simulation for the Spin Transport in Magnetic Thin Films

K. Akabli and H. T. Diep

*Laboratoire de Physique Théorique et Modélisation  
CNRS-Université de Cergy-Pontoise, UMR 8089  
2, Avenue A. Chauvin, 95302 Cergy-Pontoise Cedex - France  
E-mail: khalid.akabli@u-cergy.fr , diep@u-cergy.fr*

The magnetic phase transition is experimentally known to give rise to an anomalous temperature-dependence of the electron resistivity in ferromagnetic crystals. Phenomenological theories based on the interaction between itinerant electron spins and lattice spins have been suggested to explain these observations. We give a review here on relevant works which allowed to understand the behavior of the resistivity as a function of temperature. We also show by extensive Monte Carlo (MC) simulation the resistivity of the spin current from low- $T$  ordered phase to high- $T$  paramagnetic phase in a ferromagnetic film. We analyze in particular effects of film thickness, surface interactions and different kinds of impurities on the spin resistivity across the critical region. The origin of the resistivity peak near the phase transition is shown to stem from the existence of magnetic domains in the critical region. We also formulate a theory based on the Boltzmann's equation in the relaxation-time approximation. This equation can be solved using numerical data obtained by our simulations. We show that our theory is in a good agreement with our MC results. Comparison with experiments is discussed.

#### 1. Introduction

The behavior of the resistivity in magnetic systems has been widely studied during the last 50 years. While the resistivity in nonmagnetic systems is unanimously attributed to the effect of phonons, the origin of the spin-dependent resistivity was not clearly understood. We had to wait until de Gennes and Friedel's first explanation in 1958<sup>1</sup> which was based on the interaction between spins of conduction electrons and magnetic lattice ions. Experiments have shown that the resistivity indeed depends on

the spin orientation.<sup>2,3,4,5,6</sup> Therefore, the resistivity was expected to depend strongly on the spin ordering of the system. Experiments on various magnetic materials have found in particular an anomalous behavior of the resistivity at the critical temperature where the system undergoes the ferromagnetic-paramagnetic phase transition.<sup>3,4,5,6</sup>

The problem of spin-dependent transport has been also extensively studied in magnetic thin films and multilayers. The so-called giant magnetoresistance (GMR) was discovered experimentally twenty years ago.<sup>7,8</sup> Since then, intensive investigations, both experimentally and theoretically, have been carried out.<sup>9,10</sup> The so-called "spintronics" was born with spectacular rapid developments in relation with industrial applications. For recent overviews, the reader is referred to the reviews by Dietl<sup>11</sup> and Bibes and Barthlmy<sup>12</sup>. Theoretically, in their pioneer work, de Gennes and Friedel<sup>1</sup> have suggested that the magnetic resistivity is proportional to the spin-spin correlation. In other words, the spin resistivity should behave as the magnetic susceptibility. This explained that the resistivity singularity is due to "long-range" fluctuations of the magnetization observed in the critical region. Craig et al<sup>13</sup> in 1967 and Fisher and Langer<sup>14</sup> in 1968 criticized this explanation and suggested that the shape of the singularity results mainly from "short-range" interaction at  $T \gtrsim T_c$  where  $T_c$  is the transition temperature of the magnetic crystal. Fisher and Langer have shown in particular that the form of the resistivity cusp depends on the interaction range. An interesting summary was published in 1975 by Alexander and coworkers<sup>15</sup> which highlighted the controversial issue. To see more details on the magnetic resistivity, we quote an interesting recent publication from Kataoka.<sup>16</sup> He calculated the spin-spin correlation function using the mean-field approximation and he could analyze the effects of magnetic-field, density of conduction electron, the interaction range, etc.

Although many theoretical investigations have been carried out, to date very few Monte Carlo (MC) simulations have been performed regarding the temperature dependence of the dynamics of spins participating in the current. In our recent works,<sup>17,18</sup> we have investigated by MC simulations the effects of magnetic ordering on the spin current in magnetic multilayers. Our results are in qualitative agreement with measurements.<sup>19</sup>

The purpose of this chapter is to recall some important works which have contributed to the understanding of the mechanisms that govern the resistivity behavior of magnetic systems.

The chapter is organized as follows. Section 2 is devoted to an introduction on the spin-independent transport. Section 3 shows a background

of spin-dependent transport which will help to analyze Monte Carlo results shown later in the chapter. In section 4 we describe our model and method. Section 5 displays our results while section 6 is devoted to a semi-numerical theory based on the Boltzmann's equation. Using the results obtained with Hoshen and Kopelman's<sup>20</sup> cluster-counting algorithm, we show an excellent agreement between our theory and our Monte Carlo data. A general conclusion is given in section 7.

## 2. Spin-independent transport

### 2.1. Drude's Model

The first model describing the electron transport is the Drude's model which supposes that the conduction electrons in metals are free. The mean time between two successive collisions  $\tau$  is called relaxation time. The conductivity is written as  $\sigma = \frac{(ne^2\tau)}{m}$ , where  $n$  is the electron density,  $m$  its mass and  $e$  its charge.  $\tau$  is related to the mean electron velocity  $v_f$  by  $\tau = \frac{l_e}{v_f}$ . In this theory, the mean free path  $l_e$ , i. e. the average length travelled by an electron between two successive collisions, is supposed to be very small compared to the system dimension  $L$ . When  $l_e \simeq L$ , one has to take into account the wave nature of the electron motion. Semi-classical or quantum theories should be used.

Another interesting quantity is the phase-coherence length  $L_\phi$  below which the electron wave packets do not change their phase. At this stage it is worth to mention that when the system is only weakly disordered, i. e. ( $l_e \gg \lambda_F$ , where  $\lambda_F$  is the Fermi wave length, we can distinguish two regimes:

- 1- The ballistic regime in which the electron does not make any collision other than by the system edges. Electronic properties are then strongly dependent on the sample shape.
- 2- The diffusive regime in which the electron makes many collisions with other electrons and/or impurities, the electron motion is Brownian. This regime is what happens in most metals.

Before going to a treatment of the transport by the Boltzmann's equation, let us show how to calculate the magnetoresistance using the Drude's theory. We show in Fig. 1 the Hall's experiment realized in 1879. In the absence of an applied magnetic field, we have the Drude's relation  $\sigma_0 = \frac{(ne^2\tau)}{m}$  and the current  $j = nev$  in the permanent regime. The main idea of the Hall's

experiment was to see how the magnetic field can alter the resistivity of the metal. The setup is the following (see Fig. 1): the sample is under an applied electric field  $E_x$  and a perpendicularly applied magnetic field  $B_z$ .

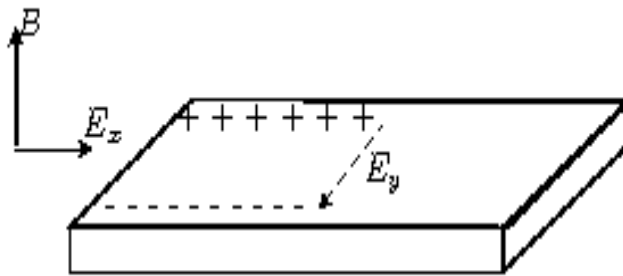


Fig. 1. Hall's experiment.

We write the following components of the current

$$\sigma_0 E_x = \frac{(eB\tau j_y)}{m} + j_x \quad (1a)$$

$$\sigma_0 E_y = -\frac{(eB\tau j_x)}{m} + j_y \quad (1b)$$

The magnetoresistance is defined as  $\rho(B) = \frac{E_x}{j_x}$ . When the Hall's field  $E_y$  is established, the current  $j_y$  is cancelled. From the first equation, we see that  $\rho(B) = \frac{E_x}{j_x} = \sigma_0^{-1}$ . This expression gives a magnetoresistance independent of  $B_z$ , contrary to experimental observation. The second relation gives the Hall's constant  $R_H = \frac{E_x}{(j_x * B)} = -\frac{1}{ne}$  which depends only on the charge density. A more detailed study shows that this is in fact a limit value of the Hall's constant.

In conclusion, the classical treatment of the electron transport cannot account for the existence of the magnetoresistance. In the following we will introduce a semi-classical treatment which will lead to a more .

## 2.2. Semi-classical theory of conduction in metals

### 2.2.1. Introduction.

In the semi-classical treatment, one uses the Bloch's theory for the electron in a periodic potential. The electron energy is therefore divided in bands separated by forbidden zones. In calculations of electronic properties, one has to use in addition the Fermi-Dirac distribution to take into account the full quantum nature of the electron. The electron velocity is given by  $v_n(k) = \frac{(\nabla_k \epsilon_n(k))}{\hbar}$  where  $n$  is the energy band index,  $k$  the wave vector and  $\epsilon_n(k)$  the electron energy.

It is interesting to note that when the electron has a wave vector on a Brillouin's zone edge, it is reflected by ions. The electron cannot travel through the crystal due to this Bragg's reflection. Other types of collisions at low temperatures include collisions by impurities, crystal defects etc which give rise to the existence of a resistance, through small, observed at low  $T$ . The collisions with phonons occur only at higher  $T$ .

### 2.2.2. Description of the model and applications

Let us show some details of the semi-classical treatment. The main purpose is to relate the electronic band structure to the transport properties.

Consider an electron at the position  $r$  with the wave vector  $k$  in the energy band  $n$ . The restrictions we impose on the time evolution of these parameters are

- $n$  does not change with time evolution. It means that the electron will stay in the same energy band.
- The evolution of  $r$  and  $k$  are given by

$$(1) \quad \frac{dr}{dt} = v_n(k) = \frac{(\nabla_k \epsilon_n(k))}{\hbar}$$

$$(2) \quad \hbar \frac{dk}{dt} = -e[E(r, t) + \frac{v_n(k) \wedge H(r, t)}{c}]$$

- The Pauli principle is obeyed. At thermal equilibrium, the electron density in a volume  $dr dk$  is given by the Fermi-Dirac distribution

$$\frac{f(\epsilon_n(k)) dk}{(4\pi^3)} = \frac{dk}{(4\pi^3)} * [exp^{\beta(\epsilon - \mu)} + 1]^{-1} \quad (2a)$$

The first condition is very strong since one has to be sure that the electric and magnetic fields are not strong enough to cause the band "breakdown". To satisfy this, we should have

- $eEa \ll [\varepsilon_{gap}(k)]^2/\varepsilon_f$ ,
- $\hbar\omega_c \ll [\varepsilon_{gap}(k)]^2/\varepsilon_f a$

where  $a$  is the lattice constant. For an electric field of  $10^{-2}V/cm$ ,  $eEa$  is of the order of  $10^{-10}eV$ . If the Fermi energy is  $1eV$ , one reaches the field limit for an energy gap smaller than  $10^{-5}eV$ . In metals, the band gap is of the order of  $10^{-1}eV$  so that this condition is easily fulfilled. However for a magnetic field such as  $\hbar\omega_c \approx 10^{-4}eV$ , the field limit for gaps of  $10^{-1}eV$  is reached at a magnetic field of the order  $10^{-2}eV$ . Such a field is often used in experiments so care should be taken to verify the second condition mentioned above. Finally the last point we should bear in mind for a semi-classical treatment is  $\lambda \gg a$  which reminds the concept of localization of wave packets.

It is worth to note that for a completely filled band or a completely empty one, there is no electron current.

### 2.2.3. Magnetoresistance

Consider a magnetic field applied along the  $z$  direction and an electric field along the  $x$  direction. One has

$$v = \frac{1}{\hbar} \frac{\partial \varepsilon(k)}{\partial k} \quad (3a)$$

$$\hbar \frac{d\vec{k}}{dt} = \frac{-e}{c} v(k) \wedge H \quad (3b)$$

Integrating from 0 to  $t$ , one has

$$\hbar \frac{d\vec{k}}{dt} = \frac{-e}{c} v(k) \wedge H - e\vec{E} \quad (4a)$$

$$\frac{c\hbar}{eH} \vec{u}_H \wedge [k(t) - k(0)] = -(r(t) - r(0)) + \left(\frac{c}{H} \vec{u}_H \wedge \vec{E}\right)t \quad (4b)$$

The energy is written as  $\overline{\varepsilon(k)} = \varepsilon(k) - \hbar \vec{k} \cdot \left(\frac{c}{H} \vec{u}_H \wedge \vec{E}\right)$ .

At the time  $t = \tau$ , the above relation becomes

$$\frac{c\hbar}{eH} \vec{u}_H \wedge \frac{[k(\tau) - k(0)]}{\tau} = -\frac{(r(\tau) - r(0))}{\tau} + \left(\frac{c}{H} \vec{u}_H \wedge \vec{E}\right) \quad (5a)$$

At this stage we should distinguish two cases:

*Case of closed orbits*

In this case the term  $(k(\tau) - k(0))$  is bounded and it becomes insignificant for large enough  $\tau$ . One then has

$$\frac{(r(\tau) - r(0))}{\tau} = \left( \frac{c}{H} \vec{u}_H \wedge \vec{E} \right) \quad (6a)$$

$$\lim_{\omega_c \tau \rightarrow 0} j_{\perp} = \frac{-nec}{H} (\vec{u}_H \wedge \vec{E}) \quad (6b)$$

This shows that the semi-classical treatment gives in the case of closed orbits the same Hall's constant given by the Drude's model.

*Case of open orbits*

In this case, the current is given by

$$\vec{j} = \sigma^{(0)} \vec{n} \cdot (\vec{n} \cdot \vec{E}) + \sigma^{(1)} \vec{E} \quad (7a)$$

where  $\vec{n}$  denotes the direction of the orbit in the real space. In the above expression, one expects for strong magnetic fields  $\sigma^{(1)}$  vanishes and  $\sigma^{(0)}$  should tend to a constant. This is easily understood because  $[k(\tau) - k(0)]$  does not have a limit with time evolution but increases with  $H$ . The application of an electric field  $\vec{E} = E^{(0)} \vec{n} + E^{(1)} \vec{n}$  will give rise to the following magnetoresistance

$$\rho = \frac{E \cdot \vec{j}}{j} = \frac{E^{(0)} \vec{n} \cdot \vec{j}}{j} \quad (8a)$$

At strong field limit,  $E^{(1)} \rightarrow 0$ , one has

$$\vec{j} = \sigma^{(0)} \vec{n} \cdot E^{(1)} + \sigma^{(1)} (\vec{n} \cdot E^{(0)} + \vec{n} \cdot \vec{E}^{(1)}) \quad (9a)$$

$$\vec{n} \cdot \vec{j} = \vec{n} \cdot E^{(0)} \cdot \sigma^{(1)} \cdot \vec{n} \quad (9b)$$

$$\rho = \frac{(\vec{n} \cdot \vec{j})^2}{\vec{n} \cdot \sigma^{(1)} \cdot \vec{n}} \quad (10a)$$

At strong field limit the conductivity  $\sigma^{(1)}$  tends to zero, so that for open orbits the magnetoresistance can infinitely increase with increasing magnetic field.

### 2.3. General equation for the transport

#### 2.3.1. Boltzmann's equation

The Boltzmann's equation describes the time evolution of the distribution function of the conducting particles. In the case of the conduction by electrons, we will denote this function by  $f(r, k, t)$ . Of course, at equilibrium,  $f(r, k, t)$  is nothing else but the Fermi-Dirac function

$$f^0 = \frac{1}{\exp[\beta(\varepsilon - \mu)] + 1} \quad (11)$$

where  $\beta = (k_B T)^{-1}$ ,  $\mu$  is the chemical potential and  $\varepsilon$  the electron energy. Let us write the following "detailed balance"

$$\frac{\partial f(r, k, t)}{\partial t} + \frac{F}{\hbar} \nabla_k(f) + v \nabla_r(f) = \left( \frac{\partial f}{\partial t} \right)_{coll} \quad (12a)$$

The left-hand side includes all possible causes of the electron diffusion and the right-hand side denotes the collision term. One supposes for the moment that electrons cannot change the energy band and their spins cannot flip. The outgoing electron number from a volume element  $dk$  is  $\left( \frac{\partial f}{\partial t} \right) \frac{dkdt}{(2\pi)^3} \omega_{k,k'} f(k)(1-f(k'))$  where  $\omega_{k,k'}$  is the transition probability from  $k$  (inside) to  $k'$  (outside). Similarly, the number of ingoing electrons after collisions is  $\left( \frac{\partial f}{\partial t} \right) \frac{dkdt}{(2\pi)^3} \omega_{k',k} f(k')(1-f(k))$ . The Boltzmann's equation is therefore rewritten as

$$\frac{\partial f(r, k, t)}{\partial t} + \frac{F}{\hbar} \nabla_k(f) + v \nabla_r(f) = \int \frac{dk'}{(2\pi)^3} \times [\omega_{k',k} f(k')(1-f(k)) - \omega_{k,k'} f(k)(1-f(k'))] \quad (13)$$

To give an explicit expression for  $\omega_{k,k'}$ , let us consider some principal sources of diffusion:

- Diffusion by impurities: Diffusion by magnetic or nonmagnetic impurities can alter the wave vector and flip the electron spin
- Diffusion by phonons: Diffusion by phonons is the main cause of the variation of the resistance with temperature
- Diffusion by electron-electron interaction: This kind of diffusion is relevant in some cases such as in pure materials and at low  $T$ .

In the case where the energy change is small when going from  $k$  to  $k'$  or vice-versa, one can use the Fermi's golden rule which was based on the perturbation theory

$$\omega_{k',k} = \frac{2\pi}{\hbar} | \langle k' | V_i | k \rangle |^2 \delta(\varepsilon_k - \varepsilon_{k'}) \quad (14a)$$

where  $V_i$  denotes the perturbative potential of the diffusing center. One has to be careful because this rule is valid only for weak potentials. One sees that

- If  $\varepsilon(k) \neq \varepsilon(k')$  then  $\omega_{k',k}$  and  $\omega_{k,k'}$  vanish
- If  $\varepsilon(k) = \varepsilon(k')$  (elastic collisions) then  $\omega_{k',k} = \omega_{k,k'}$ .

The right-hand side of Eq. (13) becomes for elastic collisions

$$\left( \frac{\partial f}{\partial t} \right)_{coll} = \int \frac{dk'}{(2\pi)^3} \omega_{k',k} [f(k') - f(k)] \quad (15a)$$

### 2.3.2. Relaxation time approximation

Suppose that the system is not far from equilibrium,  $f(k)$  is not very different from  $f^0(k)$ . Using the relaxation time approximation  $\left( \frac{\partial f}{\partial t} \right)_{coll} \simeq -\frac{f^1(k)}{\tau_k}$ , one has

$$f(k) = f^0(k) + f^1(k) \quad (16a)$$

$$\tau(k)^{-1} = \int \frac{dk'}{(2\pi)^3} \omega_{k',k} \left[ 1 - \frac{f^1(k')}{f^1(k)} \right] \quad (16b)$$

where  $f^1 \ll f^0$ . Let us give the expression of  $f^1(k)$  in the simple case where there is only an electric field as perturbation source:

$$f^1(k) = \tau(k) v_k \left( -\frac{\partial f^0}{\partial \varepsilon_k} \right) eE \quad (17a)$$

In imposing that the relaxation time depends only on  $\varepsilon_k$ , one obtains

$$\tau(k)^{-1} = \int \frac{dk'}{(2\pi)^3} \omega_{k',k} \left[ 1 - \frac{k' \cdot E}{k \cdot E} \right] \quad (18a)$$

Note that when there are several independent perturbations which yield several relaxation times, we have the following Matthiessen's rule  $\tau^{-1} = \sum_i \tau_i^{-1}$ . This expression is not always in agreement with experiments. In fact, it is difficult to prove that diffusions by different kinds of mechanisms are all independent. Therefore, it has been proposed the following generalized Matthiessen's rule  $\tau^{-1} \geq \sum_i \tau_i^{-1}$ .

### 2.3.3. Calculation of magnetoresistance

Consider the Boltzmann's equation with both electric and magnetic fields

$$\vec{v} \cdot e \vec{E} \left( \frac{\partial f^0}{\partial \varepsilon} \right) + \frac{e}{\hbar} (\vec{v} \wedge \vec{B}) \cdot \vec{\nabla}_k f^1 = -\frac{f^1}{\tau} \quad (19a)$$

For  $\vec{B} = (0, 0, B_z)$  and  $\vec{E} = (E_x, E_y, 0)$ , one obtains

$$j_x = \frac{ne^2}{m} \left[ \left\langle \frac{\tau}{1 + \omega_c^2 \tau^2} \right\rangle + \left\langle \frac{\omega_c \tau^2}{1 + \omega_c^2 \tau^2} \right\rangle * \left\langle \frac{\tau}{1 + \omega_c^2 \tau^2} \right\rangle^{-1} \right] E_x \quad (20a)$$

where  $\omega_c = \frac{-eB}{m}$  (cyclotron frequency). If  $\omega_c \tau \ll 1$ , one has

$$j_x = \frac{ne^2}{m} \left[ \langle \tau \rangle - \omega_c^2 \langle \tau^3 \rangle + \omega_c^2 * \frac{\langle \tau^2 \rangle^2}{\langle \tau \rangle} \right] E_x \quad (21a)$$

The variation due to the magnetic field is

- If  $\omega_c \tau \ll 1$  then  $\frac{\nabla \sigma}{\sigma} = \frac{[-\omega_c^2 \langle \tau \rangle \langle \tau^3 \rangle - \langle \tau^2 \rangle^2]}{\langle \tau \rangle^2}$
- If  $\omega_c \tau \gg 1$  then  $\frac{\nabla \sigma}{\sigma} = \frac{[\langle \tau^{-1} \rangle^{-1} - \langle \tau \rangle]}{\langle \tau \rangle}$

To close this section, we emphasize that we have shown some historic treatments of the transport phenomenon with no spin dependence. The Boltzmann's equation was introduced to allow some developments in the later part of this chapter. The magnetoresistance has been calculated without spin effects. These will be considered in the following section.

## 3. Spin-dependent transport

### 3.1. Introduction

As said in section 1, the spin-dependent transport has been spectacularly developed in the last 20 years. This is due to the so-called spintronics which uses the properties of the spin current in magnetic devices for memory storages and magnetic sensors in general.<sup>7,8,9</sup>

Already in the sixties, Fert and Campbell have shown the existence of spin-dependent conduction.<sup>2</sup> The conduction depends on the magnetic ordering of the lattice: when the itinerant electron has its spin parallel to the lattice spins, it can go through the system. Otherwise, it will suffer a strong resistivity. As a consequence, in a ferromagnetic metal with a Curie temperature  $T_c$ , the spin resistivity is very small for  $T < T_c$  and very

large for  $T > T_c$ . Near  $T_c$ , the shape of the resistivity depends on several ingredients which are specific for each material. For example, in the case of transition metals (Fe, Co, Ni) one observes a huge peak of the resistivity  $\rho$  at  $T_c$ .

Let us confine our discussion on the temperature dependence of the spin resistivity. The field dependence will not be developed here. The first theory which has attempted to explain the anomaly behavior of the resistivity at  $T_c$  was due to Kasuya.<sup>21</sup> He affirmed that the variation of the magnetic resistivity below  $T_c$  can be described by spin-dependent collisions. In this theory, Kasuya neglected the effect of short-range interaction between spins. Using the spin-spin correlation function for all distances, de Gennes and Friedel<sup>1</sup> have shown that the spin fluctuations could be the origin of the resistivity anomaly at  $T_c$ . This result was criticized by Fisher and Langer<sup>14</sup> on the ground that long-range correlation cannot explain the peak because the mean free path is finite in this temperature region. Among other works which have treated this question one can mention that of Alexander et al.<sup>15</sup> and Kataoka.<sup>16</sup> We will return to these works after showing some experimental data.

### **3.2. Experimental results**

Let us mention here some experiments on the resistivity of several materials showing different behaviors as a function of  $T$ . Measurements performed by Legvold and al.<sup>22</sup> on Gadolinium of hexagonal close-packed structure with ferromagnetic state showed a change of slope near  $T_c \simeq 16 \pm 1$  K. They have isolated effects of impurities smaller than 0,02% of Mg, 0,03% of Ca, 0,15% of Sm and about 0,02% of Fe. Similar measurements on Dysprosium have confirmed the observed behavior of Gd. It is noted that there exists a temperature range where the resistivity is constant (Fig. 2).

Other experiments made by Kawatra and al.<sup>23</sup> on some binary compounds of the type  $RX_2$  such as  $GdCo_2$  (Curie temperature of about 393 K) showed the same behavior. The authors were able to distinguish contributions from phonons and impurities by using the first derivative of the resistivity with respect to  $T$ . It is noted that the peak is very fine and the resistivity is asymmetric around  $T_c$  (Fig. 3).

Another interesting work was due to Schwerer and Cuddy<sup>3</sup> who showed a complete experiment on Ni and Fe. They showed interesting effects of impurities on the spin resistivity. Using the Matthieussen's rule, they showed the resistivity coming from magnetic and nonmagnetic impurities as a func-

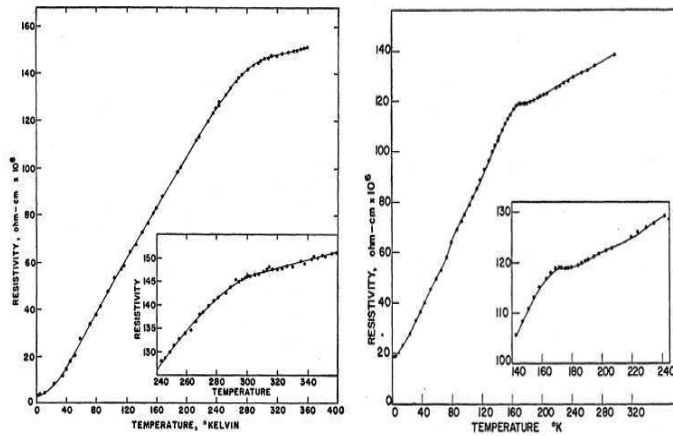


Fig. 2. Resistivity of Gadolinium (right) and Dysprosium (left) taken from Ref. 22.

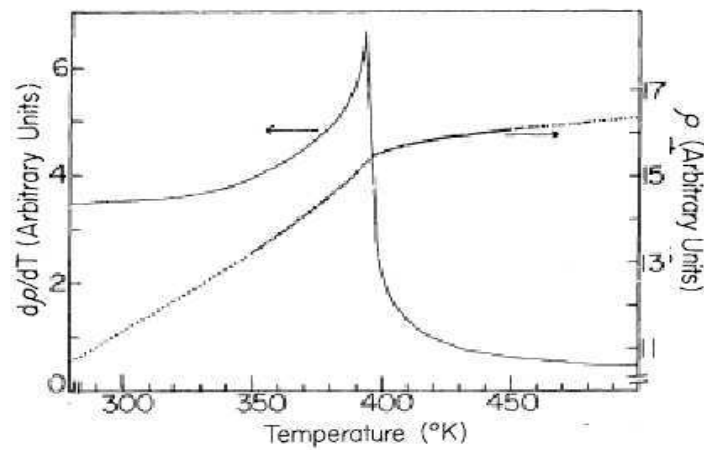


Fig. 3. Resistivity  $\rho(T)$  and its derivative  $d\rho(T)/dT$  for  $GdCo_2$  taken from Ref. 23.

tion of  $T$ . Various behaviors have been then observed: for Ni one finds a deflection with 1% Fe impurities, a peak with 1% Cu impurities, and a huge peak with 1% Cr impurities, etc...(Fig. 4)

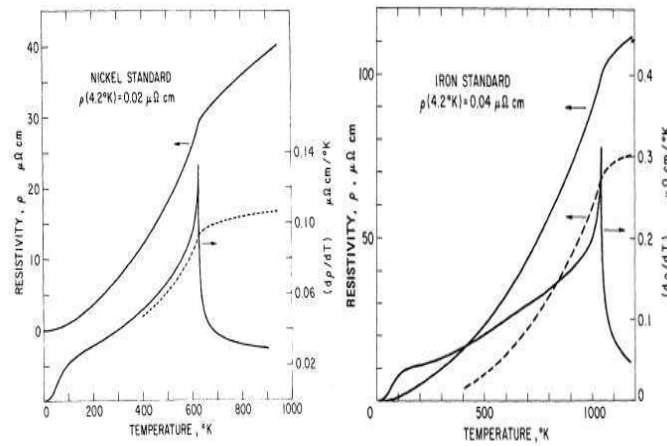


Fig. 4. Resistivity  $\rho(T)$  and its derivative  $d\rho(T)/dT$  obtained for Ni (left) and Fe (right) taken from Ref. 3.

### 3.3. Kasuya's model

In transition metals (Fe, Co, Ni,...) and in rare-earth elements (Eu, Gd, ...), the resistance depends strongly on  $T^{24}$ (see Fig. 5). In the study of the

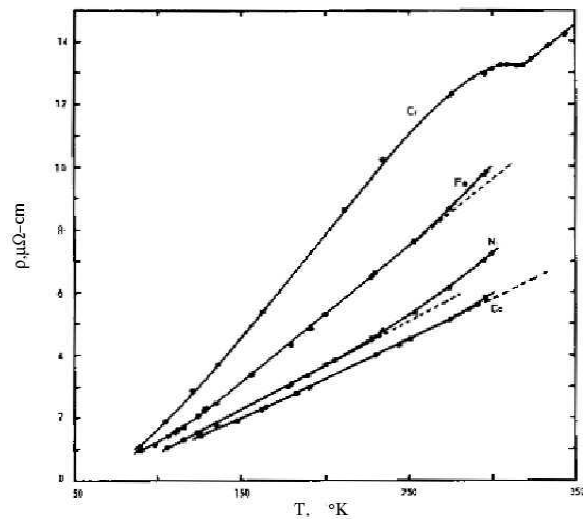


Fig. 5. Resistivity of some transition metals taken from Ref. 24.

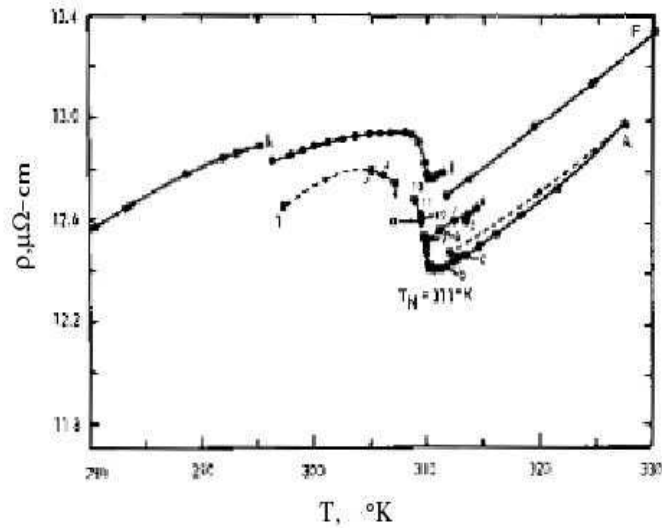


Fig. 6. Resistivity of Cobalt near the Neel temperature  $T_{Neel}$  taken from Ref. 24.

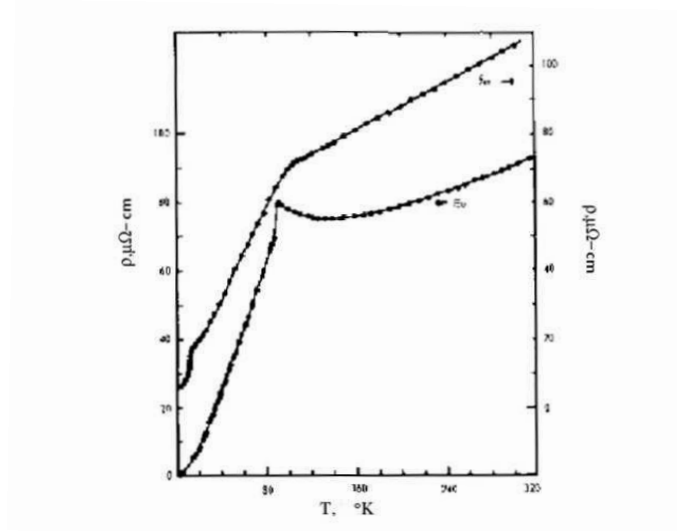


Fig. 7. Resistivity of Europium (atomic number 63) taken from Ref. 24.

phononic resistivity ( $\rho_{ph}$ ), one distinguishes two regimes

- $T \ll \Theta_D$  (Debye temperature), the relaxation time varies as  $T^{-5}$
- $T \gg \Theta_D$ , the relaxation time varies as  $T^{-1}$

We note that  $\theta_D$  corresponds to a temperature beyond which all normal phonon modes are excited, the Debye approximation is no more valid.

The resistivity thus obeys a  $T^5$ -law at low  $T$  and a  $T$ -law at high  $T$ . However, one observes experimentally<sup>3,4</sup> another change of slope near  $T_c$  for ferromagnets or near  $T_N$  (Neel temperature) for antiferromagnets (see Fig. 5 and Fig. 6). The origin of the resistivity anomaly has been discussed by many authors among them one can mention Mott.<sup>25</sup> According to him, we have to take account the inter band transition because of the following fact: the effective mass of  $s$  electrons is small with respect to that of  $d$  electrons so the main conduction is made by  $s$  electrons. However, the density of states of the  $d$  band is much larger than that of the  $s$  band so the transition from  $s$  to  $d$  band is more frequent than that between  $s$  and  $s$  states. The resistivity depends thus on the magnetic properties of  $d$  band.

It seems however that this mechanism cannot fully explain the resistivity anomaly in transition metals near the Curie temperature.

T. Kasuya<sup>21</sup> gave another argument: i) in the case of rare-earth elements, the atomic configuration is characterized by  $f$  shells with very narrow bands. The transition process between bands suggested by Mott is in fact very rare and it cannot explain the resistivity peak (Fig. 7), ii) the Mott's process cannot explain the sharp and abrupt decrease of the resistance at  $T_c$ .

T. Kasuya proposed an alternative: one has to use the effect of the exchange interactions between  $s$ ,  $d$  and  $f$  electrons according to the system under consideration. This observation allowed to understand qualitatively the resistivity behavior: at low  $T$  where ferromagnetic ordering is perfect the resistivity is zero and in the paramagnetic state, the resistivity is constant.

Kasuya used the Boltzmann's equation [Eq. (13)] with a diffusion probability proportional to the exchange integral. Solving this equation by mean-

field approximation, he obtained

$$\rho = \left( \frac{3\pi m^*2}{Ne^2\hbar^2} \right) (S - \sigma)(S + \sigma + 1) \frac{J_{eff}^2}{\varepsilon_0} ohm, \quad (22a)$$

In the expression [Eq. (22a)],  $\sigma$  is the mean value of the spin component  $S_z$  and  $J_{eff}$  the effective exchange integral.<sup>21</sup>

Note that the mean-field approximation may not be adequate to predict correctly the resistivity behavior in particular its decrease above  $T_c$ .

### 3.4. Model by de Gennes and Friedel

The fact that the resistivity is related to the spin-spin interaction led de Gennes and Friedel to use the spin-spin correlation to describe the resistivity behavior.

To study explicitly they used a model where the spins  $S$  of the magnetic ions are localized at the lattice sites. The interaction between two neighbors is given by  $2JS_R.S_R'$ . The itinerant electrons interact with the lattice spins by a contact Hamiltonian

$$H_I = \sum_{R,p} G\delta(R - R_p)S_R.S_p \quad (23a)$$

The determination, by a Born approximation, of the diffusion section  $\sigma$  assuming elastic collisions allows to get an expression for the resistivity in the case without correlation. One has then

$$\frac{d\sigma}{d\Omega} = \sigma_0 \frac{S(S+1) - \langle S^z \rangle^2}{S(S+1)} \quad (24)$$

$$\frac{\tau_0}{\tau} = 1 - \frac{\langle S^z \rangle^2}{S(S+1)} \quad (25)$$

These relations show the dependence of the resistance on the order parameter  $\langle S^z \rangle$ . As Kasuya, de Gennes and Friedel<sup>1</sup> explained only in a phenomenological manner the constant resistivity behavior above  $T_c$ .

We determine by the Green's function method the mean value  $\langle S^z \rangle$

appearing in Eq. (24) for spin 1/2 as follows<sup>26,27,28</sup>

$$G_{i,j} = \langle S_i^+ \cdot S_j^- \rangle, \quad (26a)$$

$$i\hbar \frac{dG_{i,j}}{dt} = \langle [S_i^+, S_j^-] \rangle \delta(t, t') - \langle \langle [H, S_i^+](t); S_j^-(t') \rangle \rangle, \quad (26b)$$

$$H = -\frac{J}{2} \sum_{l,p} S_l \cdot S_p \quad (26c)$$

Solving Eq. (26b) with a Tyablikov decoupling, we obtain the magnon dispersion relation  $\epsilon(k)$ . The magnetization is given by

$$\langle S^z \rangle = \frac{1}{2} - \frac{2 \langle S^z \rangle}{N} \sum_k \frac{1}{e^{\beta\hbar\epsilon(k)} - 1} \quad (27)$$

We can solve this equation self-consistently to obtain  $\langle S^z \rangle$  as a function of  $T$ . Replacing this into Eq. (25) we plot in Fig. 8 the inverse of the relaxation time which is proportional to the spin resistance. A comparison

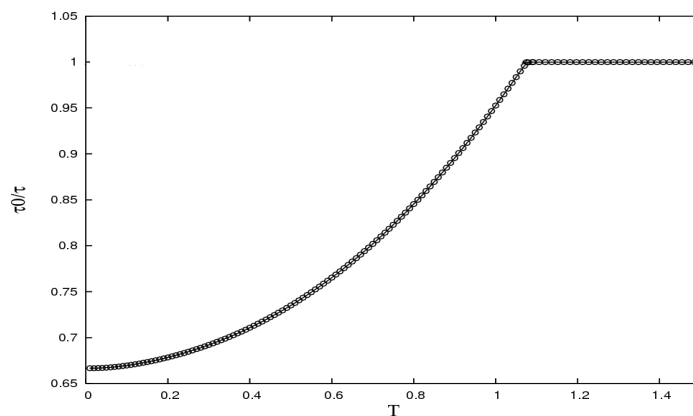


Fig. 8. Eq. (25) estimated by using the Green's function method with  $\frac{J}{k_B T_c} = 1$  and  $B = 0$ .

with experiments on Gd, AuMn<sup>1</sup> shows clearly a disagreement at low  $T$ . Now, if one uses the correlation function as the diffusion probability, one can correctly describe the resistivity behavior at  $T_c$  and beyond. Taking into account correlations at all distances, de Gennes and Friedel<sup>1</sup> found

$$\frac{\tau_0}{\tau} = \frac{1}{4} \int_0^2 \frac{x^3 dx}{1 - \frac{T_c \sin(xk_0d)}{T}} \quad (28a)$$

where  $x^2 = 2(1 - \cos(\theta))$ . This new expression is displayed in Fig. 9 where one observes the decrease of the resistivity as  $T$  increases above  $T_c$  in agreement with experimental results shown in Fig. 7 for the case of Europium (atomic number 63). In the same figure, we also display the resistance for

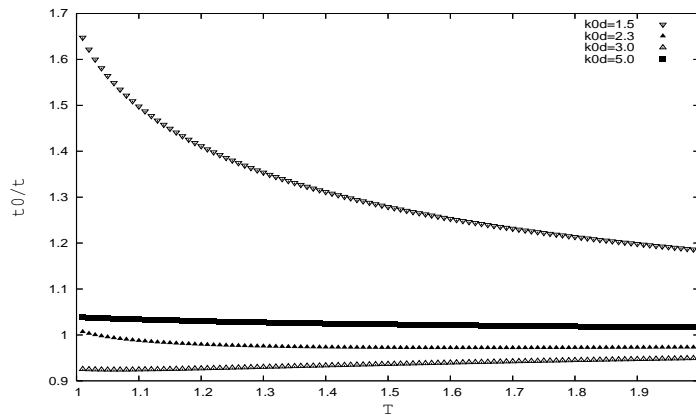


Fig. 9. Relaxation time, Eq. (28a), versus  $T$  for different values of  $k_0d$ .

different  $k_0d$ , where  $k_0$  is the wave vector and  $d$  the lattice constant. For  $k_0d \ll \pi$  (resp.  $k_0d \geq \pi$ ), the effect of the correlation is strong (resp. weak). This allows to distinguish two types of behavior for  $T > T_c$ :

- Resistivity is constant if the correlation is weak
- Resistivity decreases with increasing  $T$  if the correlation is strong.

### 3.5. Model by Fisher and Langer

The point raised by Fisher and Langer concerned the correlation used in the calculation of the resistivity at  $T_c$ .<sup>14,29</sup> De Gennes and Friedel included long-ranged fluctuations near  $T_c$  using an extension of the Ornstein-Zernike approximation.<sup>30</sup> The result near  $T_c$  is in disagreement with experiments on Ni.<sup>13</sup> Fisher and Langer suggested to use only short-range fluctuations for the calculation of the resistivity at  $T_c$ . The reason was that long-range

correlations were not compatible with the finite mean free path  $l$  of the conduction electrons in this region of temperature. In addition, they suggested to use a screening function to reduce the long-range character of the correlation

$$p(R) = \exp(-R/l) \quad (29a)$$

$$\frac{\tau_0}{\tau} = \sum_{s=0}^{\infty} \nu_s f(R_s) p(R_s) \Gamma(R_s), \quad (29b)$$

In the expression of the relaxation time, Eq. (29b), the first term corresponds to the number of spins in a cell of radius  $R_s$  and the second term is the following decreasing function

$$f(R) = \frac{1}{4k_F^4 R} \frac{d^2}{dR^2} \left( \frac{\cos(2k_f R) - 1}{R} \right) \quad (30a)$$

The last term in Eq. (29b) is the spin-spin correlation function. Taking  $p(R) \equiv 1$ , we show this function in Fig. 10 as a function of reduced temperature for different  $Ka$  ( $K$ : wave vector,  $a$ : lattice constant). At small  $Ka$  (i.e long-range) the peak is very high at large values of  $Ka$  (short-range) it is lowered. In addition, this calculation shows that the peak position is slightly higher than  $T_c$ .

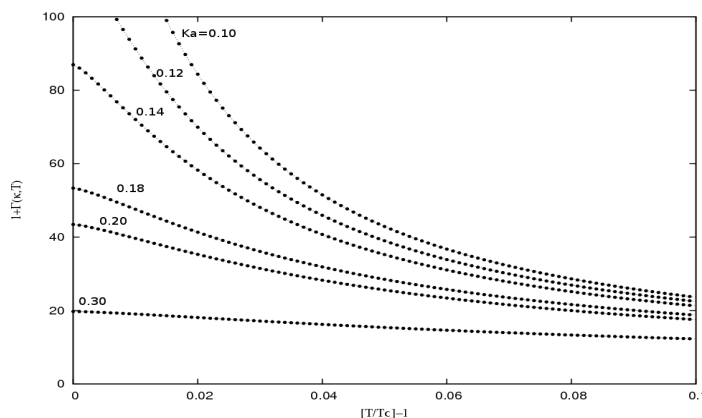


Fig. 10. Spin-spin correlation function versus temperature for different values of  $Ka$ .

### 3.6. Kataoka's model

Kataoka<sup>16</sup> has built a model which combined main ingredients of the previous ones. The model was made for transition metals, it has a root in the  $s-d$  model suggested by Kasuya describing the diffusion of the itinerant  $s$  electron by the localized  $d$  electrons. Kataoka used the collision probability and the concept of correlation function introduced by de Gennes-Friedel and Fisher-Langer. He solved the Boltzmann's equation with a mean-field approximation. His results show explicitly the effects of several important ingredients:

- How the mean free path due to nonmagnetic diffusion is affected by the temperature near  $T_c$
- How the spin transport is affected by an applied magnetic field for up- and down-spin states
- How the itinerant spin concentration affects the behavior of the resistivity near  $T_c$
- How the stability of the ferromagnetic phase modifies the resistivity.

The Hamiltonian used is written as

$$\begin{aligned}
 H_{ele} = & \sum_{k,\sigma} \epsilon_{k,\sigma} a_{k,\sigma}^{\dagger} a_{k,\sigma} \\
 & - \frac{J_{sd}}{N} \sum_{k,\sigma} [\bar{S}_z(q) (a_{k+q\uparrow}^{\dagger} a_{k\uparrow} \\
 & - a_{k+q\downarrow}^{\dagger} a_{k\downarrow}) + S_-(q) a_{k+q\uparrow}^{\dagger} a_{k\downarrow} + S_+(q) a_{k+q\downarrow}^{\dagger} a_{k\uparrow}] \quad (31)
 \end{aligned}$$

where  $J_{sd}$  is exchange interaction  $s-d$ ,  $S(q)$  the Fourier transform of the lattice spin  $S_i$  and  $\epsilon_{k,\sigma}$  the energy of an electron of spin ( $\sigma_z = 1$ (resp.  $-1$ ) in the mean-field approximation. We have

$$\epsilon_{k,\sigma} = \frac{\hbar^2 k^2}{2m_{\sigma}^*} - J_{sd} \langle S_z \rangle \sigma_z - \frac{1}{2} g \mu_B H_{ext} \sigma_z. \quad (32a)$$

The Boltzmann's equation defined in Eq. (13) can be generalized to take into account the spin nature and its possible flip. One can write the collision

term as

$$\begin{aligned}
\left(\frac{df_\sigma(k)}{dt}\right)_c &= \left(\frac{J_{sd}^2}{\hbar N^2}\right) \sum_{k'} [f_\sigma(k')(1 - f_\sigma(k))\omega(k'\sigma, k\sigma) \\
&\quad - f_\sigma(k)(1 - f_\sigma(k'))\omega(k\sigma, k'\sigma)] \\
&\quad + \left(\frac{J_{sd}^2}{\hbar N^2}\right) \sum_{k'} [f_{\sigma^-}(k')(1 - f_\sigma(k))\omega(k'\sigma^-, k\sigma) \\
&\quad - f_\sigma(k)(1 - f_{\sigma^-}(k'))\omega(k\sigma, k'\sigma^-)] \quad (33)
\end{aligned}$$

The diffusion probabilities  $\omega(k\sigma, k'\sigma)$  and  $\omega(k\sigma, k'\sigma^-)$  related to the correlation function can be expressed as

$$\omega(k\sigma, k'\sigma) = \left(\frac{J_{sd}^2}{\hbar N^2}\right) \int \langle \bar{S}_z(k - k', 0) \bar{S}_z(k' - k, t) \rangle e^{iT_{\sigma\sigma}(k, k')t} dt, \quad (34a)$$

$$\omega(k\sigma, k'\sigma^-) = \left(\frac{J_{sd}^2}{\hbar N^2}\right) \int \langle S_{\sigma-\sigma}(k - k', 0) S_{\sigma\sigma^-}(k' - k, t) \rangle e^{iT_{\sigma\sigma^-}(k, k')t} dt, \quad (34b)$$

where " $T_{\sigma\sigma^-}(k, k') = \epsilon_{k\sigma} - \epsilon_{k'\sigma^-}$ " is the transferred energy of an electron during the transition  $|k\sigma\rangle \rightarrow |k'\sigma^- \rangle$  and  $S_{\uparrow\downarrow}$  (resp.  $S_{\downarrow\uparrow}$ ) represent  $S_-$  (resp.  $S_+$ ).

By using the relaxation time approximation and by supposing a situation very close to equilibrium, Kataoka expressed the spin resistivity as a function of relaxation times  $\tau_{\downarrow}$  and  $\tau_{\uparrow}$  with and without spin flip

$$\rho = \frac{3}{2e^2} \left[ \frac{\langle\langle \tau_{\uparrow} \rangle\rangle}{m_{\uparrow}^*} + \frac{\langle\langle \tau_{\downarrow} \rangle\rangle}{m_{\downarrow}^*} \right]^{-1} \quad (35)$$

At this stage, it is worth to express the collision probability using the spin-spin correlation function incorporating the so-called stability parameter of the ferromagnetic state. This parameter contains the second-nearest neighbor interaction  $J_2$  which can destroy the ferromagnetic state if it is large and antiferromagnetic (the ground state becomes then helimagnetic)

$$\begin{aligned}
H_{spin} &= -\frac{1}{N} \sum_q (\bar{S}_z(q) \bar{S}_z(-q) \\
&\quad + \frac{1}{2} [S_+(q) S_-(-q) + S_-(q) S_+(-q)]) \\
&\quad - \sum_i (2J^{eff}(0) \langle S_z \rangle + H_{ext}) S_{iz} \quad (36)
\end{aligned}$$

where

$$J^{eff}(q) = J_1 \cos\left(\frac{aq}{2}\right) - J_2 \cos(aq) \quad (37)$$

Note that  $J_1$  and  $J_2$  are positive and  $a$  is the lattice constant. The first term gives rise to the ferromagnetic ordering while the second term describes the antiferromagnetic interaction between next-nearest neighbors which is in competition with  $J_1$ . When  $J_2/J_1 \geq 0.25$ , a helimagnetic structure takes place.

The parallel susceptibility in mean-field approximation is

$$\chi_{\parallel} = \frac{NS^2(g\mu_B)^2 B'_S}{k_B T - 2ZJS^2 B'_S} \quad (38)$$

where  $B_S = B_s(g\mu_B\beta SH_m)$  is the Brillouin function and  $B'_s$  its first derivative.  $H_m$  represents the last term of the Hamiltonian. The correlation function is

$$\begin{aligned} \langle \bar{S}_z(q)\bar{S}_z(-q) \rangle &= \frac{NS^2 k_B T B'_S}{k_B T_c [T/T_c + (a\kappa_0^{\parallel})^2] - 2S^2 J^{eff}(q) B'_S} \\ \langle S_x(q)S_x(-q) \rangle &= \langle S_y(q)S_y(-q) \rangle = \\ &= \frac{NSk_B T B_S}{g\mu_B H_m [1 + (a\kappa_0^{\perp})^2] - 2S J^{eff}(q) B_S} \end{aligned} \quad (39)$$

where  $\kappa_0$  is a phenomenological parameter describing the range of the spin-spin correlation. The parameter  $\kappa_0$  will allow to test the hypothesis of Fisher and Langer on the importance of short-ranged correlation.

Solving the Boltzmann's equation for paramagnetic phase gives an expression very different from that of Fisher and Langer<sup>14</sup>:

$$\rho = \rho_0 S(S+1)(W/\epsilon_F)r(t) \quad (40)$$

$$r(t) = (t - t_c + t_s)[1 - t \ln(1 + t^{-1})] \quad (41)$$

$$t = t_s \left( \frac{T}{T_c} - 1 \right) + t_c \quad (42)$$

$$t_s = (2ak_F\xi)^{-2} \quad (43)$$

$$t_c = (2k_F l_0)^{-2} \quad (44)$$

where  $W$  represents the width of the conduction band and  $t_s(\xi)$  is a parameter which controls the instability of the ferromagnetic state. The value of  $t_c(l_0)$  shows that the mean free path is in fact finite.

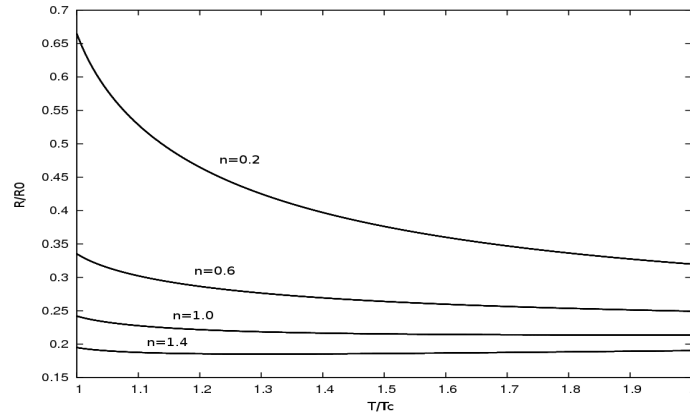


Fig. 11. Normalized resistivity versus temperature for different electron densities.

Figure 11 shows the effect of the density of itinerant electrons on the resistivity. We observe that the peak height increases with decreasing density. This behavior is closely related to the spin-spin correlation shown in Fig. 9. We will return to this point later.

The effect of the finite mean free path  $l_0$  phenomenologically introduced in the expression of the correlation function is shown in Fig. 12. One observes that as  $l_0$  decreases the peak height decreases. One sees that for weak  $l_0$  combined with strong  $\xi$  will suppress the peak of the resistivity.

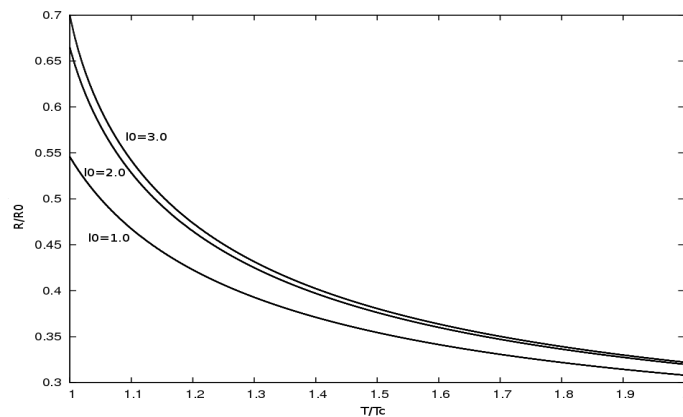


Fig. 12. Normalized resistivity versus temperature for different values of  $l_0$ .

Figure 13 shows the effect of the instability of the ferromagnetic state. The more the ferromagnetic state is unstable, the higher the resistivity peak becomes. In addition, the peak position moves slightly from the initial  $T_c$ .

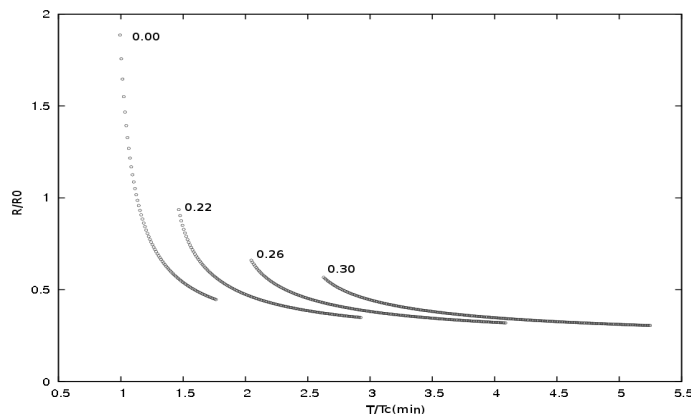


Fig. 13. Normalized resistivity versus temperature for different values of  $\xi$ .

To summarize, we say that the model by Kataoka includes all ingredients which affect the resistivity behavior. In spite of the fact that the solution of this model was obtained by a mean-field approximation, the results are in qualitative agreement with experiments provided that appropriate values for parameters have to be used for each studied material.

### 3.7. Conclusion

In spite of the effort of several researchers, there exists at present no single theory able to explain results on the magnetic resistivity in various materials and under different situations. One finds that the different theories discussed above can be applied in different cases: while the models by de Gennes-Friedel et by Fisher-Langer work properly in ferromagnetic metals, the model of Haas<sup>31</sup> is more suitable for magnetic semiconductors and the model by Suezaki and Mori<sup>32</sup> improved by Kasuya and Kondo<sup>33</sup> is better suited for antiferromagnets. Another important point emphasized by Alexander et al. in a review<sup>15</sup> is that one has to be careful about attempts to compare experimental data with theoretical critical exponents associated with the resistivity's anomaly at  $T_c$ : while a good agreement is observed in the temperature range  $10^{-4} < |T - T_c|/T_c < 10^{-1}$  for ferromagnetic metals,

there is no such agreement in rare-earth elements specially in the critical region where fluctuations were neglected in different theories.

#### 4. Our model and method

Due to a large number of parameters which play certainly important roles at various degrees in the behavior of the spin resistivity, it is difficult to treat all parameters at the same time. The first question is of course whether the explanation provided by de Gennes and Friedel can be used in some kinds of material and that by Fisher and Langer can be applied in some other kinds of material. In other words, we would like to know the validity of each of these two arguments. We will return to this point in subsection 5.6. The second question concerns the effects of magnetic or non-magnetic impurities on the resistivity. Note that in 1970, Schwerer and Cuddy<sup>3</sup> have shown and compared their experimental results with the different existing theories to understand the impurity effect on the magnetic resistivity. However, the interpretation was not clear enough at the time to understand the real physical mechanism lying behind. The third question concerns the effects of the surface on the spin resistivity in thin films. These questions are treated hereafter.

We study here by extensive MC simulations the transport of itinerant electrons travelling in a ferromagnetic thin film. We use the Ising model and take into account various interactions between lattice spins and itinerant spins. We show that the magnetic resistivity depends on the lattice magnetic ordering. We analyze this behavior by using a new idea: instead of calculating the spin-spin correlation, we calculate the distribution of clusters in the critical region. We show that the resistivity depends on the number and the size of clusters of opposite spins. We establish also a Boltzmann's equation which can be solved using numerical data for the cluster distribution obtained by our MC simulation.

We take into account (i) interactions between itinerant and lattice spins, (ii) interactions between itinerant spins themselves and (iii) interactions between lattice spins. We include a thermodynamic force due to the gradient of itinerant electron concentration, an applied electric field and the effect of a magnetic field. For impurities, we take the Rudermann-Kittel-Kasuya-Yoshida (RKKY) interaction between them. We describe hereafter the details of our model.

#### 4.1. Model

We consider here a ferromagnetic thin film. We use the Ising model and the face-centered cubic (FCC) lattice with size  $N_x \times N_y \times N_z$ . Periodic boundary conditions (PBC) are used in the  $xy$  planes. Spins localized at FCC lattice sites are called "lattice spins" hereafter. They interact with each other through the following Hamiltonian

$$\mathcal{H}_l = -J \sum_{\langle i,j \rangle} \mathbf{S}_i \cdot \mathbf{S}_j, \quad (45)$$

where  $\mathbf{S}_i$  is the Ising spin at lattice site  $i$ ,  $\sum_{\langle i,j \rangle}$  indicates the sum over every nearest-neighbor (NN) spin pair  $(\mathbf{S}_i, \mathbf{S}_j)$ ,  $J (> 0)$  being the NN interaction.

In order to study the spin transport in the above system, we consider a flow of itinerant spins interacting with each other and with the lattice spins. The interaction between itinerant spins is defined as follows,

$$\mathcal{H}_m = - \sum_{\langle i,j \rangle} K_{i,j} \mathbf{s}_i \cdot \mathbf{s}_j, \quad (46)$$

where  $\mathbf{s}_i$  is the itinerant Ising spin at position  $\vec{r}_i$ , and  $\sum_{\langle i,j \rangle}$  denotes a sum over every spin pair  $(\mathbf{s}_i, \mathbf{s}_j)$ . The interaction  $K_{i,j}$  depends on the distance between the two spins, i.e.  $r_{ij} = |\vec{r}_i - \vec{r}_j|$ . A specific form of  $K_{i,j}$  will be chosen below. The interaction between itinerant spins and lattice spins is given by

$$\mathcal{H}_r = - \sum_{\langle i,j \rangle} I_{i,j} \mathbf{s}_i \cdot \mathbf{S}_j, \quad (47)$$

where the interaction  $I_{i,j}$  depends on the distance between the itinerant spin  $\mathbf{s}_i$  and the lattice spin  $\mathbf{S}_j$ . For the sake of simplicity, we assume the same form for  $K_{i,j}$  and  $I_{i,j}$ , namely,

$$K_{i,j} = K_0 \exp(-r_{ij}) \quad (48)$$

$$I_{i,j} = I_0 \exp(-r_{ij}) \quad (49)$$

where  $K_0$  and  $I_0$  are constants.

#### 4.2. Method

The procedure used in our simulation is described as follows. First we study the thermodynamic properties of the film alone, i.e. without itinerant spins,

using Eq. (45). We perform MC simulations to determine quantities as the internal energy, the specific heat, layer magnetizations, the susceptibility, ... as functions of temperature  $T$ .<sup>34</sup> From these physical quantities we determine the critical temperature  $T_c$  below which the system is in the ordered phase. We show in Fig. 14 the lattice magnetization versus  $T$  for  $N_z = 8$ ,  $N_x = N_y = 20$ .

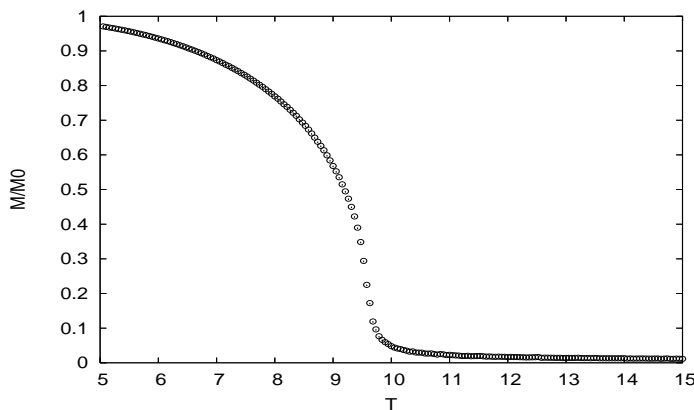


Fig. 14. Lattice magnetization versus temperature  $T$  for  $N_z = 8$ .  $T_c$  is  $\simeq 9.58$  in unit of  $J = 1$ .

Once the lattice has been equilibrated at  $T$ , we inject  $N_0$  itinerant spins into the system. The itinerant spins move into the system at one end, travel in the  $x$  direction, escape the system at the other end to reenter again at the first end under the PBC. Note that the PBC are used to ensure that the average density of itinerant spins remains constant with evolving time (stationary regime). The dynamics of itinerant spins is governed by the following interactions:

- i) an electric field  $\mathbf{E}$  is applied in the  $x$  direction. Its energy is given by

$$\mathcal{H}_E = -e\mathbf{E} \cdot \mathbf{v}, \quad (50)$$

where  $\mathbf{v}$  is the velocity of the itinerant spin,  $e$  its charge;

- ii) a chemical potential term which depends on the concentration of itinerant spins ("concentration gradient" effect). Its form is given by

$$\mathcal{H}_c = Dn(\mathbf{r}), \quad (51)$$

where  $n(\mathbf{r})$  is the concentration of itinerant spins in a sphere of radius  $D_2$  centered at  $\mathbf{r}$ .  $D$  is a constant taken equal to  $K_0$  for simplicity;

iii) interactions between a given itinerant spin and lattice spins inside a sphere of radius  $D_1$  [Eq. (47)];

iv) interactions between a given itinerant spin and other itinerant spins inside a sphere of radius  $D_2$  [Eq. (46)].

Let us consider the case without an applied magnetic field. The simulation is carried out as follows: at a given  $T$  we calculate the energy of an itinerant spin by taking into account all the interactions described above. Then we tentatively move the spin under consideration to a new position with a step of length  $v_0$  in an arbitrary direction. Note that this move is immediately rejected if the new position is inside a sphere of radius  $r_0$  centered at a lattice spin or an itinerant spin. This excluded space emulates the Pauli exclusion principle in the one hand, and the interaction with lattice phonons on the other hand. If the new position does not lie in a forbidden region of space, then the move is accepted with a probability given by the standard Metropolis algorithm.<sup>34</sup>

To study the case with impurities, we replace randomly a number of lattice spins  $S$  by impurity spins  $\sigma$ . The impurities interact with each other via the RKKY interaction as follows

$$\mathcal{H}_I = - \sum_{\langle i,j \rangle} L(r_i, r_j) \sigma_i \cdot \sigma_j \quad (52)$$

where

$$L(r_i, r_j) = L_0 \cos(2k_F |r_i - r_j|) / |r_i - r_j|^3 \quad (53)$$

$L_0$  being a constant and  $k_F$  the Fermi wave number of the lattice. The impurity spins also interact with NN lattice spins. However, to reduce the number of parameters, we take this interaction equal to  $J = 1$  as that between NN lattice spins [see Eq. (45)] with however  $\sigma \neq S$ . We will consider here two cases  $\sigma = 2$  and  $\sigma = 0$ .

## 5. Monte Carlo Results

### 5.1. Simple case

We let  $N_0$  itinerant spins travel through the system several thousands times until a steady state is reached. The parameters we use in most calculations, except otherwise stated (for example, in subsection 5.3 for  $N_z$ ) are  $s = S = 1$  and  $N_x = N_y = 20$  and  $N_z = 8$ . Other parameters are  $D_1 = D_2 = 1$  (in unit of the FCC cell length),  $K_0 = I_0 = 2$ ,  $L_0 = 17$ ,  $N_0 = 8 \times 20^2$  (namely one itinerant spin per FCC unit cell),  $v_0 = 1$ ,  $k_F = (\frac{\pi}{a})(\frac{n_0}{2})^{1/3}$ ,  $r_0 = 0.05$ .

At each  $T$  the equilibration time for the lattice spins lies around  $10^6$  MC steps per spin and we compute statistical averages over  $10^6$  MC steps per spin. Taking  $J = 1$ , we find that  $T_c \simeq 9.58$  for the critical temperature of the lattice spins (see Fig. 14).

We define the resistivity  $\rho$  as

$$\rho = \frac{1}{n}, \quad (54)$$

where  $n$  is the number of itinerant spins crossing a unit area perpendicular to the  $x$  direction per unit of time.

We show in Figs. 15 and 16 the simulation results for different thicknesses. In all cases, the resistivity  $\rho$  is very small at low  $T$ , undergoes a huge peak in the ferromagnetic-paramagnetic transition region, decreases slowly at high  $T$ .

We point out that the peak position of the resistivity follows the variation of critical temperature with changing thickness (see Fig. 15) and  $\rho$  at  $T \gtrsim T_c$  becomes larger when the thickness decreases. This is due to the fact that surface effects tend to slow down itinerant spins. We return to this point in the next subsection.

The temperature of resistivity's peak at a given thickness is always slightly higher than the corresponding  $T_c$ .

## 5.2. Our interpretation

Let us discuss the temperature dependence of  $\rho$  shown in Fig. 16:

i) First,  $\rho$  is very low in the ordered phase. We can explain this by the following argument: below the transition temperature, there exists a single large cluster of lattice spins with some isolated "defects" (i. e. clusters of antiparallel spins), so that any itinerant spin having the parallel orientation goes through the lattice without hindrance. The resistance is thus very small but it increases as the number and the size of "defect" clusters increase with increasing temperature.

ii) Second,  $\rho$  exhibits a cusp at the transition temperature. We present here three interpretations of the existence of this cusp. Note that these different pictures are not contradictory with each other. They are just three different manners to express the same physical mechanism. The first picture consists in saying that the cusp is due to the critical fluctuations in the phase transition region. We know from the theory of critical phenomena that there is a critical region around the transition temperature  $T_c$ . In this region, the mean-field theory should take into account critical fluctuations.

The width of this region is given by the Ginzburg criterion. The limit of this "Ginzburg" region could tally with the resistivity's peak and Ginzburg temperature.<sup>15</sup> The second picture is due to Fisher-Langer<sup>14</sup> and Kataoka<sup>16</sup> who suggested that the form of peak is due mainly to short-range spin-spin correlation. These short-range fluctuations are known to exist in the critical region around the critical point. The third picture comes from our MC simulation<sup>17</sup> which showed that the resistivity's peak is due to the formation of antiparallel-spin clusters of sizes of a few lattice cells which are known to exist when one enters the critical region. Note in addition that the cluster size is now comparable with the radius  $D_1$  of the interaction sphere, which in turn reduces the height of potential energy barriers. We have checked this interpretation by first creating an artificial structure of alternate clusters of opposite spins and then injecting itinerant spins into the system. We observed that itinerant spins do advance indeed more slowly than in the completely disordered phase (high- $T$  paramagnetic phase). We have next calculated directly the cluster-size distribution as a function of  $T$  using the Hoshen-Kopelman's algorithm.<sup>20</sup> The result confirms the effect of clusters on the spin conductivity. We will show in the next section a cluster distribution for the film studied here.

iii) Third,  $\rho$  is large in the paramagnetic phase and decreases with an increasing temperature. Above  $T_c$  in the paramagnetic phase, the spins become more disordered as  $T$  increases: small clusters will be broken into single disordered spins, so that there is no more energy barrier between successive positions of itinerant spins on their trajectory. The resistance, though high, is decreasing with increasing  $T$  and saturated as  $T \rightarrow \infty$ .

iv) Let us touch upon the effects of varying  $D_1$  and  $D_2$  at a low temperatures.  $\rho$  is very small at small  $D_1$  ( $D_1 < 0.8$ ): this can be explained by the fact that for such small  $D_1$ , itinerant spins do not "see" lattice spins in their interaction sphere so they move almost in an empty space. The effect of  $D_2$  is on the other hand qualitatively very different from that of  $D_1$ :  $\rho$  is very small at small  $D_2$  but it increases to very high value at large  $D_2$ . We conclude that both  $D_1$  and  $D_2$  dominate  $\rho$  at their small values. However, at large values, only  $D_2$  has a strong effect on  $\rho$ . This effect comes naturally from the criterion on the itinerant spins concentration used in the moving procedure. Also, we have studied the effect of the electric field  $E$  both above and below  $T_c$ . The low-field spin current verifies the Ohm regime. These effects have been also observed in magnetic multilayer.<sup>17</sup> The reader is referred to that work for a detailed presentation of these points.

Let us show now the effect of magnetic field on  $\rho$ . As it is well known,

when a magnetic field is applied on a ferromagnet, the phase transition is suppressed because the magnetization will never tend to zero. Critical fluctuations are reduced, the number of clusters of antiparallel spins diminishes. As a consequence, we expect that the peak of the resistivity will be reduced and disappears at high fields. This is what we observed in simulations. We show results of  $\rho$  for several fields in Fig. 17.

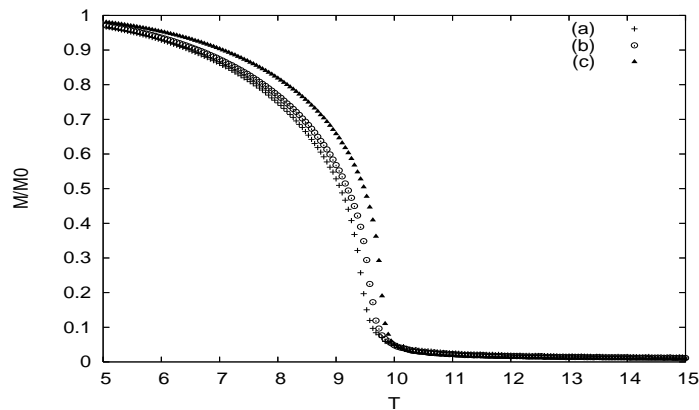


Fig. 15. Lattice magnetization versus temperature  $T$  with different thicknesses ( $N_z$ ) of the film: crosses, void circles and black triangles indicate data for  $N_z=5$ , 8 and bulk, respectively.  $T_c(\text{bulk}) \simeq 9.79$ ,  $T_c(N_z = 8) \simeq 9.58$  and  $T_c(N_z = 5) \simeq 9.47$ .

### 5.3. Effect of surface

The picture suggested above on the physical mechanism causing the variation of the resistivity helps to understand the surface effect shown here. Since the surface spins suffer more fluctuations due to the lack of neighbors, we expect that surface lattice spins will scatter more strongly itinerant spins than the interior lattice spins. The resistivity therefore should be larger near the surface. This is indeed what we observed. The effect however is very small in the case where only a single surface layer is perturbed. To enhance the surface effect, we have perturbed a number of layers near the surface: we considered a sandwich of three films: the middle film of 4 layers is placed between two surface films of 5 layers each. The in-plane interaction between spins of the surface films is taken to be  $J_s$  and that of the middle film is  $J$ . When  $J_s = J$  one has one homogeneous 14-layer film. We have simulated the two cases where  $J_s = J$  and  $J_s = 0.2J$  for sorting out the surface effect.

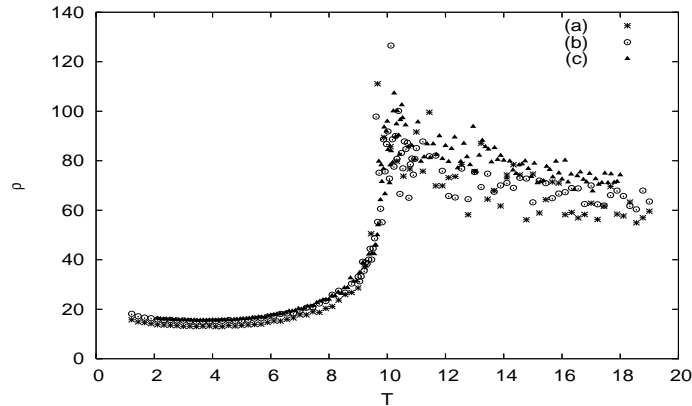


Fig. 16. Resistivity  $\rho$  in arbitrary unit versus temperature  $T$  for different film thicknesses. Crosses (a), void circles (b) and black triangles (c) indicate data for bulk,  $N_z=8$  and 5, respectively.

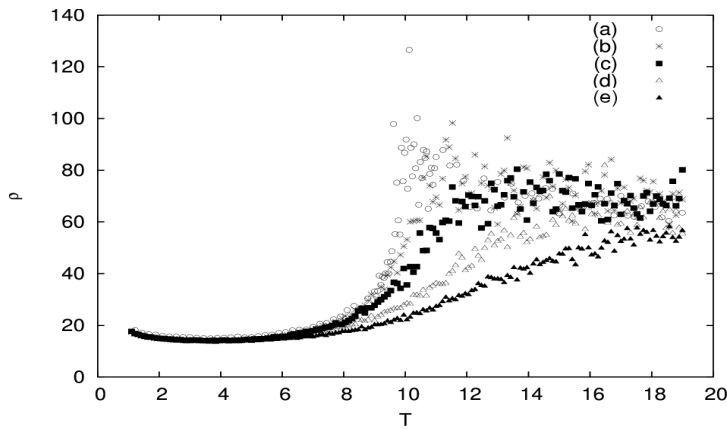


Fig. 17. Resistivity  $\rho$  in arbitrary unit versus temperature  $T$ , for different magnetic fields. Void circles, stars, black rectangles, void triangles and black triangles indicate, respectively, data for (a)  $B = 0$ , (b)  $B = 0.1J$ , (c)  $B = 0.3J$ , (d)  $B = 1J$  and (e)  $B = 2J$ .

In the absence of itinerant spins, the lattice spins undergo a single phase transition at  $T_c \simeq 9.75$  for  $J_s = J$ , and two transitions when  $J_s = 0.2J$ : the first transition occurs at  $T_1 \simeq 4.20$  for "surface" films and the second at  $T_2 \simeq 9.60$  for "middle" film. This is seen in Fig. 18 where the magnetization of the surface films drops at  $T_1$  and the magnetization of the middle film remains up to  $T_2$ . The susceptibility has two peaks in the case  $J_s = 0.2J$ . The resistivity of this case is shown in Fig. 19: at  $T < T_1$  the whole system

is ordered,  $\rho$  is therefore small. When  $T_1 \leq T \leq T_2$  the surface spins are disordered while the middle film is still ordered: itinerant spins encounter strong scattering in the two surface films, they "escape", after multiple collisions, to the middle film. This explains the peak of the surface resistivity at  $T_1$ . Note that already far below  $T_1$ , a number of surface itinerant spins begin to escape to the middle film, making the resistivity of the middle film to decrease with increasing  $T$  below  $T_1$  up to  $T_2$ , as seen in Fig. 19. Note that there is a small shoulder of the total resistivity at  $T_1$ . In addition, in the range of temperatures between  $T_1$  and  $T_2$  the spins travel almost in the middle film with a large density resulting in a very low resistivity of the middle film. For  $T > T_2$ , itinerant spins flow in every part of the system.

#### 5.4. *Effect of impurity*

In this subsection, we take back  $N_x = N_y = 20$  and  $N_z = 8$ .

##### 5.4.1. *Magnetic impurities*

To treat the case with impurities, we replace randomly a number of lattice spins  $S$  by impurity spins  $\sigma = 2$ . We suppose an RKKY interaction between impurity spins [see Eq. (52)]. Figure 20 shows the lattice magnetization for several impurity concentrations. We see that critical temperature  $T_c$  increases with magnetic impurity's concentration. We understand that large-spin impurities must reinforce the magnetic order.

In Figs. 21, 22 and 23, we compare a system without impurity to systems with respectively 1 and 2 and 5 percents of impurities. The temperature of resistivity's peak is a little higher than the critical temperature and we see that the peak height increases with increasing impurity concentration (see Fig. 23). This is easily explained by the fact that when large-spin impurities are introduced into the system, additional magnetic clusters around these impurities are created in both ferromagnetic and paramagnetic phases. They enhance therefore  $\rho$ .

##### 5.4.2. *Non-magnetic impurities*

For the case with non-magnetic impurities, we replace randomly a number of lattice spins  $S$  by zero-spin impurities  $\sigma = 0$ . Figures 24, 25 and 26 show, respectively, the lattice magnetizations and the resistivities for non-magnetic impurity concentrations 1% and 5%. We observe that non-magnetic impurities reduce the critical temperature and the temperature

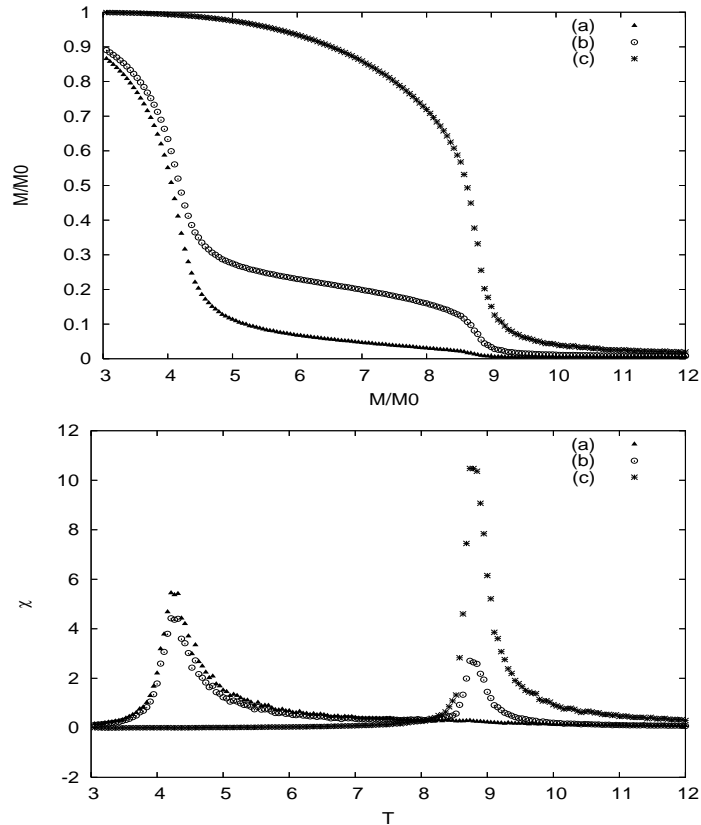


Fig. 18. Upper figure: Magnetization versus  $T$  in the case where the system is made of three films: the first and the third have 5 layers with a weaker interaction  $J_s$ , while the middle has 4 layers with interaction  $J = 1$ . We take  $J_s = 0.2J$ . Black triangles: magnetization of the surface films, stars: magnetization of the middle film, void circles: total magnetization. Lower figure: Susceptibility versus  $T$  of the same system as in the upper figure. Black triangles: susceptibility of the surface films, stars: susceptibility of the middle films, void circles: total susceptibility. See text for comments.

of the resistivity's peak. This can be explained by the fact that the now "dilute" lattice spins has a lower critical temperature so that the scattering of itinerant spins by lattice-spin clusters should take place at lower temperatures.

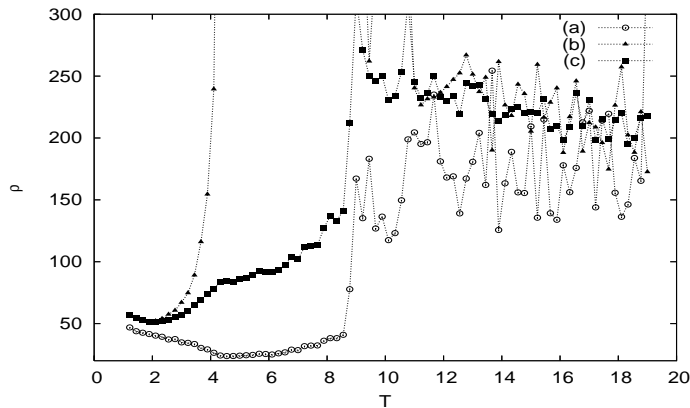


Fig. 19. Resistivity  $\rho$  in arbitrary unit versus  $T$  of the system described in the previous figure's caption. Black triangles: resistivity of the surface films, void circles: resistivity of the middle film, black squares: total resistivity. See text for comments.

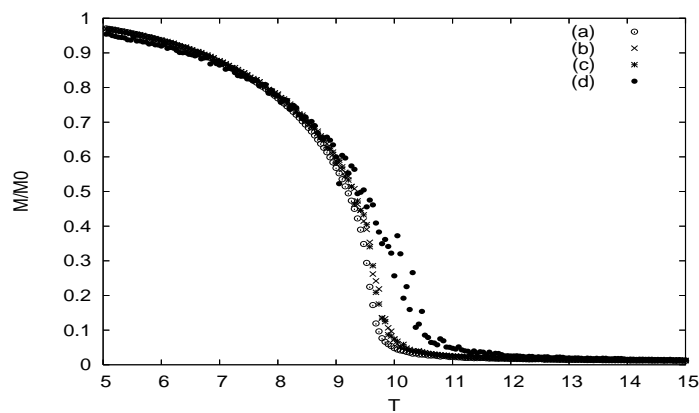


Fig. 20. Lattice magnetization versus temperature  $T$  with different concentrations of magnetic impurities  $C_I$ . Void circles, crosses, stars and black diamonds indicate, respectively, data for (a)  $C_I = 0\%$ , (b)  $C_I = 1\%$ , (c)  $C_I = 2\%$  and (d)  $C_I = 5\%$ .

### 5.5. Effect of electron concentration

Let us show here the effect of the concentration of itinerant electrons. We have shown above the results for  $n_0 = 1/4$ . According to the theory of Kataoka,<sup>16</sup> the stronger the electron density is the smaller the resistivity peak becomes. Physically, larger density causes stronger screening effect on the spin-spin correlation. As a result, one expects that the correlation is

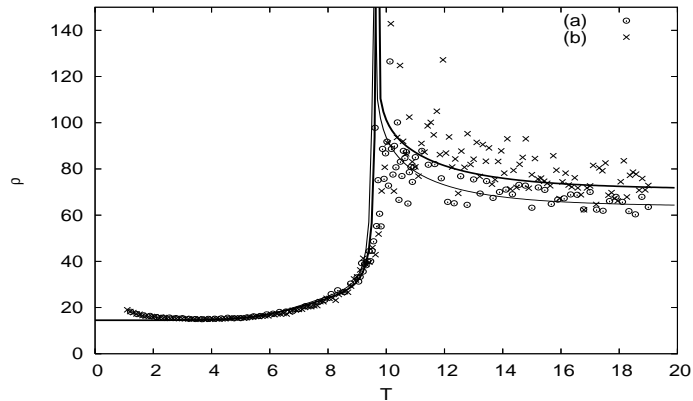


Fig. 21. Resistivity  $\rho$  in arbitrary unit versus temperature  $T$ . Two cases are shown: without (a) and with 1% (b) of magnetic impurities (void circles and crosses, respectively). Our result using the Boltzmann's equation is shown by the continuous curves (see sect. IV): thin and thick lines are for (a) and (b), respectively. Note that  $T_c \simeq 9.68$  for  $C_I = 1\%$ .

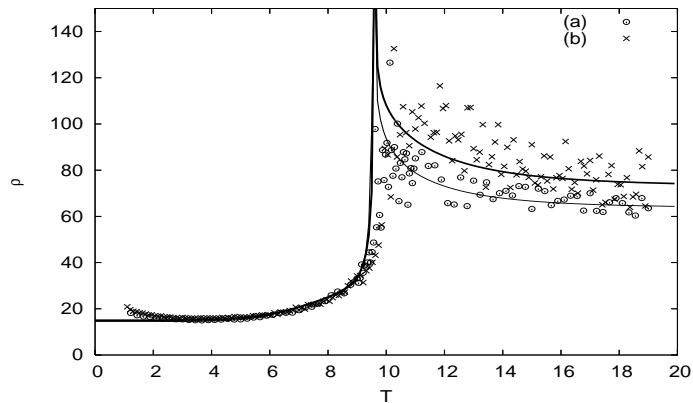


Fig. 22. Resistivity  $\rho$  in arbitrary unit versus temperature  $T$ . Two cases are shown: without and with 2% of magnetic impurities (void circles and crosses, respectively). Our result using the Boltzmann's equation is shown by the continuous curves (see sect. IV): thin and thick lines are for (a) and (b), respectively.  $T_c \simeq 9.63$  for 2% .

shorter in the system. Therefore, the peak height will be reduced as we have seen above while discussing on the models by Fisher and Langer and by Kataoka. What about the results of the simulations? To answer this question, we have carried out calculations with  $n_0 = 1/8$  and  $n_0 = 1/2$

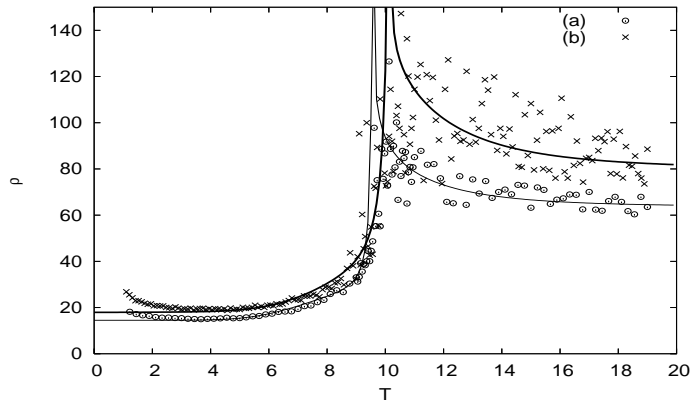


Fig. 23. Resistivity  $\rho$  in arbitrary unit versus temperature  $T$ . Two cases are shown: without (a) and with 5% of magnetic impurities (b) (void circles and crosses, respectively). Our result using the Boltzmann's equation is shown by the continuous curves (see sect. IV): thin and thick lines are for (a) and (b), respectively.  $T_c \simeq 10.21$  for 5%.

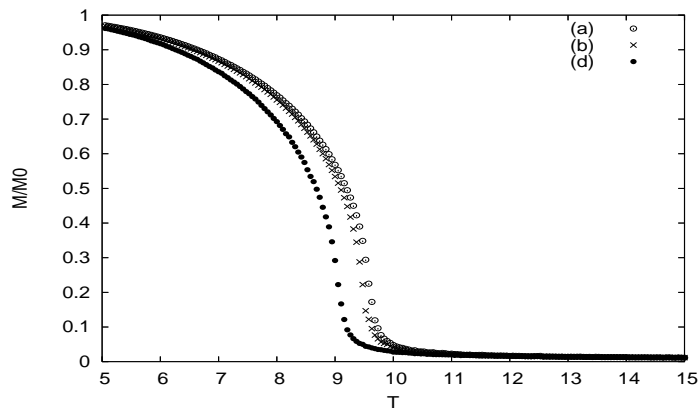


Fig. 24. Lattice magnetization versus temperature  $T$  for different concentrations of non-magnetic impurities: (a)  $C_I = 0\%$  (void circles), (b)  $C_I = 1\%$  (crosses) and (c)  $C_I = 5\%$  (black diamonds).

for comparison with results shown above for  $n_0 = 1/4$ . We show in Fig. 27 the susceptibility for  $n_0 = 1/8$ ,  $n_0 = 1/4$  and  $n_0 = 1/2$ . We observe that the larger density reduces the peak height of the susceptibility. Since the resistivity is related to the susceptibility, we conclude that it will have the same behavior under the effect of electron concentration (see discussion below).

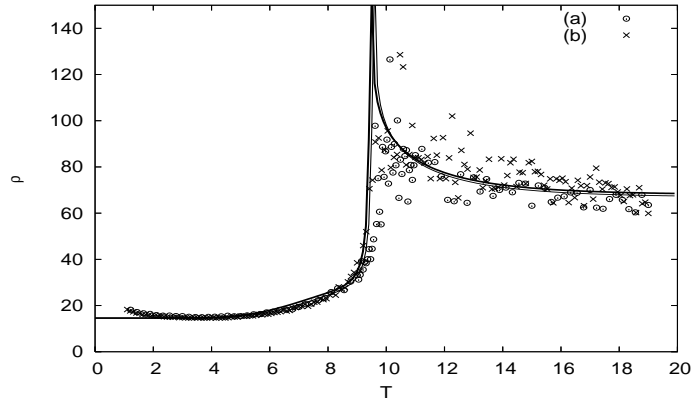


Fig. 25. Resistivity  $\rho$  in arbitrary unit versus temperature  $T$  for two cases: without (a) and with 1% of non-magnetic impurities (b) (void circles and crosses, respectively). Our result using the Boltzmann's equation is shown by the continuous curves (see sect. IV): thin and thick lines are for (a) and (b), respectively.

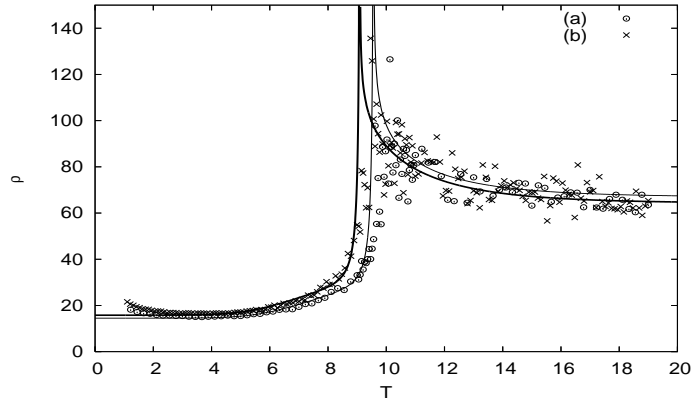


Fig. 26. Resistivity  $\rho$  in arbitrary unit versus temperature  $T$  for two cases: without (a) and with 5% of non-magnetic impurities (b) (void circles and crosses, respectively). Our result using the Boltzmann's equation is shown by the continuous curves (see sect. IV): thin and thick lines are for (a) and (b), respectively.

### 5.6. Discussion

De Gennes and Friedel<sup>1</sup> have shown that the resistivity  $\rho$  is related to the spin correlation  $\langle \mathbf{S}_i \cdot \mathbf{S}_j \rangle$ . They have suggested therefore that  $\rho$  behaves as the magnetic susceptibility  $\chi$ . However, unlike the susceptibility which diverges at the transition, the resistivity observed in many experiments

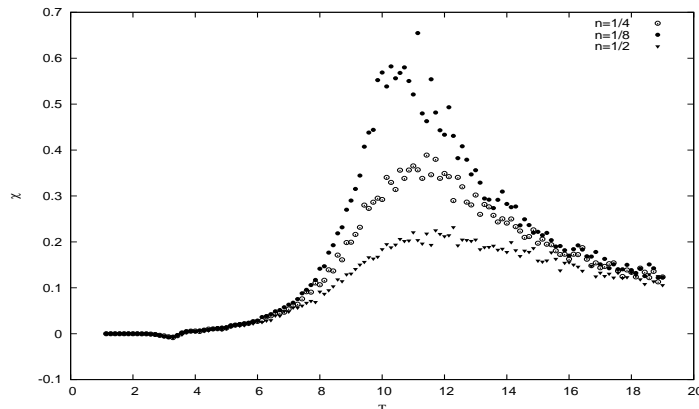


Fig. 27. Susceptibility for  $n_0 = 1/8$ ,  $n_0 = 1/4$  and  $n_0 = 1/2$ . Note that the peak is smaller for higher concentration. See text for comments.

goes through a finite maximum, i. e. a cusp, without divergence. To explain this, Fisher and Langer<sup>14</sup> and then Kataoka<sup>16</sup> have shown that the cusp is due to short-range correlation. This explanation is in agreement with many experimental data but not all (see Ref. <sup>15</sup> for review on early experiments).

Let us recall that  $\langle E \rangle \propto \sum_{i,j} \langle \mathbf{S}_i \cdot \mathbf{S}_j \rangle$  where the sum is taken over NN (or short-range) spin pairs while  $T\chi \propto \langle (\sum_i \mathbf{S}_i)^2 \rangle = \sum_{i,j} \langle \mathbf{S}_i \cdot \mathbf{S}_j \rangle$  where the sum is performed over *all* spin pairs. This is the reason why short-range correlation yields internal energy and long-range correlation yields susceptibility.

Roughly speaking, if  $\langle \mathbf{S}_i \cdot \mathbf{S}_j \rangle$  is short-ranged, then  $\rho$  behaves as  $\langle E \rangle$  so that the temperature derivative of the resistivity, namely  $d\rho/dT$ , should behave as the specific heat with varying  $T$ . Recent experiments have found this behavior (see for example Ref. <sup>5</sup>).

Now, if  $\langle \mathbf{S}_i \cdot \mathbf{S}_j \rangle$  is long-ranged, then  $\rho$  behaves as the magnetic susceptibility as suggested by de Gennes and Friedel.<sup>1</sup> In this case,  $\rho$  undergoes a divergence at  $T_c$  as  $\chi$ . One should have therefore  $d\rho/dT > 0$  at  $T < T_c$  and  $d\rho/dT < 0$  at  $T > T_c$ . In some experiments, this has been found in for example in magnetic semiconductors (Ga,Mn)As<sup>6</sup> (see also Ref. <sup>15</sup> for review on older experiments). We think that all systems are not the same because of the difference in interactions, so one should not discard a priori one of these two scenarios.

In this chapter, we suggest another picture to explain the cusp: when  $T_c$  is approached, large clusters of up (resp. down) spins are formed in the

critical region above  $T_c$ . As a result, the resistance is much larger than in the ordered phase: itinerant electrons have to steer around large clusters of opposite spins in order to go through the entire lattice. Thermal fluctuations are not large enough to allow the itinerant spin to overcome the energy barrier created by the opposite orientation of the clusters in this temperature region. Of course, far above  $T_c$ , most clusters have a small size, the resistivity is still quite large with respect to the low- $T$  phase. However,  $\rho$  decreases as  $T$  is increased because thermal fluctuations are more and more stronger to help the itinerant spin to overcome energy barriers.

What we have found here is a peak of  $\rho$ , not a peak of  $d\rho/dT$ . So, our resistivity behaves as the susceptibility although the peak observed here is not sharp and no divergence is observed. We believe however that, similar to commonly known disordered systems, the susceptibility peak is broadened more or less because of the disorder. The disorder in the system studied here is due the lack of periodicity in the positions of moving itinerant spins.

## 6. Simple cluster theory

In this paragraph, we show a theory based on the Boltzmann's equation in the relaxation-time approximation. To solve completely this equation, we shall need some numerical data from MC simulations for the cluster sizes as will be seen below. Using these data, we show that our MC result of resistivity is in a good agreement with this theory.

Let us formulate now the Boltzmann's equation for our system. When we think about the magnetic resistivity, we think of the interaction between lattice spins and itinerant spins. We recognize immediately the important role of the spin-spin correlation function in the determination of the mean free-path. If we inject through the system a flow of spins "polarized" in one direction, namely "up", we can consider clusters of "down" spins in the lattice as "defect clusters", or as "magnetic impurities", which play the role of scattering centers. We therefore reduce the problem to the determination of the number and the size of defect clusters. For our purpose, we use the Boltzmann's equation with uniform electric field but without gradient of temperature and gradient of chemical potential. We write the equation for  $f$ , the Fermi-Dirac distribution function of itinerant electrons, as

$$\left(\frac{\hbar\mathbf{k}\cdot e\mathbf{E}}{m}\right)\left(\frac{\partial f^0}{\partial \varepsilon}\right) = \left(\frac{\partial f}{\partial t}\right)_{coll}, \quad (55)$$

where  $\mathbf{k}$  is the wave vector,  $e$  and  $m$  the electronic charge and mass,  $\varepsilon$  the

electron energy. We use the following relaxation-time approximation

$$\left(\frac{\partial f_k}{\partial t}\right)_{coll} = -\left(\frac{f_k^1}{\tau_k}\right), \quad f_k^1 = f_k - f_k^0, \quad (56)$$

where  $\tau_k$  is the relaxation time. Supposing elastic collisions, i. e.  $k = k'$ , and using the detailed balance we have

$$\left(\frac{\partial f_k}{\partial t}\right)_{coll} = \frac{\Omega}{(2\pi)^3} \int w_{k',k} (f_{k'}^1 - f_k^1) dk', \quad (57)$$

where  $\Omega$  is the system volume,  $w_{k',k}$  the transition probability between  $k$  and  $k'$ . We find with Eq. (56) and Eq. (57) the following well-known expression

$$\begin{aligned} \left(\frac{1}{\tau_k}\right) &= \frac{\Omega}{(2\pi)^3} \int w_{k',k} (1 - \cos \theta) \\ &\quad \times \sin \theta k'^2 dk' d\theta d\phi, \end{aligned} \quad (58)$$

where  $\theta$  and  $\phi$  are the angles formed by  $\mathbf{k}'$  with  $\mathbf{k}$ , i. e. spherical coordinates with  $z$  axis parallel to  $\mathbf{k}$ .

We use now for Eq. (58) the "Fermi golden rule" and we obtain

$$\begin{aligned} \left(\frac{1}{\tau_k}\right) &= \frac{\Omega m}{\hbar^3 2\pi k} \int | \langle k' | V | k \rangle |^2 (1 - \cos \theta) \sin \theta \\ &\quad \times \delta(k' - k) k'^2 dk' d\theta \end{aligned} \quad (59)$$

We give for the potential  $V$  the following expression which reminds the form of the interactions (48)-(49)

$$V = V_0 \exp\left(\frac{-r}{\xi(T)}\right), \quad (60)$$

where  $\xi(T)$  is the size of the defect cluster and  $V_0$  a constant. We resolve Eq. (59) with Eq. (60) and we have the following expression

$$\left(\frac{1}{\tau_k}\right) = \left(\frac{32V_0^2 \Omega m k \pi}{\hbar^3}\right) \int \frac{\sin \theta (1 - \cos \theta)}{(K^2 + \xi^{-2})^3} d\theta, \quad (61)$$

where  $K = |\vec{k} - \vec{k}'|$  is given by

$$K = |\vec{k} - \vec{k}'| = k[2(1 - \cos \theta)]^{1/2}, \quad (62)$$

Integrating Eq. (61) we obtain

$$\begin{aligned} \left(\frac{1}{\tau_k}\right) &= \frac{32(V_0 \Omega)^2 m \pi}{(2k\hbar)^3} n_c \xi^2 \\ &\quad \times \left[1 - \frac{1}{1 + 4k^2 \xi^2} - \frac{4k^2 \xi^2}{(1 + 4k^2 \xi^2)^2}\right] \end{aligned} \quad (63)$$

where  $n_c$  is the number of clusters of size  $\xi$ . We integrate Eq. (63) for the interval  $[0, k_F]$  and we obtain finally

$$\left(\frac{1}{\tau}\right) = \frac{(4V_0\Omega m)^2}{\pi(\hbar)^{3/2}} n_c \xi^2 \times \left[ \frac{1}{1 + (2k_F\xi)^2} + \ln(1 + (2k_F\xi)^2) - 1 \right] \quad (64)$$

Note that although the relaxation time  $\tau$  is averaged over all states in the Fermi sphere, i. e. states at  $T = 0$ , its temperature dependence comes from the parameters  $\xi$  and  $n_c$ . These will be numerically determined in the following. If we know  $\tau$  we can calculate the resistivity by the Drude expression

$$\rho_m = \frac{m}{ne^2} \frac{1}{\tau}, \quad (65)$$

Let us use now the Hoshen-Kopelman's algorithm<sup>20</sup> to determine the mean value of  $\xi$  and the number of the cluster's mean size, for different temperatures. The Hoshen-Kopelman's algorithm allows to regroup into clusters spins with equivalent value for  $T < T_c$  or equivalent energy for  $T > T_c$ . Using this algorithm during our MC simulation at a given  $T$ , we obtain a "histogram" representing the number of clusters as a function of the cluster size. For temperature  $T$  below  $T_c$ , we call a cluster a group of parallel spins surrounded by opposite spins, and for  $T$  above  $T_c$  a cluster is a group of spins with the same energy. At a given  $T$ , we estimate the average size  $\xi$  using the histogram as follows: calling  $N_i$  the number of spins in the cluster and  $P_i$  the probability of the cluster deduced from the histogram, we have

$$\xi = \frac{\sum_i N_i P_i}{\sum_i P_i}, \quad (66)$$

In doing this we obtain  $\xi$  for the whole temperature range. We note that we can fit the cluster size  $\xi$  with the following formula

$$\xi = A|T_c - T|^{\nu/3}, \quad (67)$$

where  $\nu$  is a fitting parameter and  $A$  a constant. These parameters are different for  $T < T_c$  and  $T > T_c$ . Figure 28 and Figure 29 show the average size and the average number of cluster versus temperature. To simplify our approach we consider that the cluster's geometry is a sphere with radius  $\xi$ . Note that due to the fact that our fitting was made separately for  $T < T_c$  and  $T > T_c$ , no effort has been made for the matching at  $T = T_c$  exactly, but this does not affect the behavior discussed below.

We distinguish hereafter temperatures below and above  $T_c$  in establishing our theory. We write

$$T < T_c \left[ \begin{array}{l} \rho_m = \rho_0(1 + C_{inf}n_c\xi^2[-1 + \frac{1}{1 + (2k_F\xi)^2} \\ + \ln(1 + (2k_F\xi)^2)]), \\ \xi = (\frac{3A_{inf}}{16\pi})^{1/3}(T_c - T)^{\nu_{inf}/3}, \\ n_c = (\frac{B_{inf}}{2\alpha\pi}) \times \exp[\frac{-(T - T_G)^2}{2\alpha^2}]. \end{array} \right. \quad (68)$$

$$T > T_c \left[ \begin{array}{l} \rho_m = \rho_\infty(1 + C_{sup}n_c\xi^2[-1 + \frac{1}{1 + (2k_F\xi)^2} \\ + \ln(1 + (2k_F\xi)^2)]), \\ \xi = (\frac{3A_{sup}}{16\pi})^{1/3}(T - T_c)^{\nu_{sup}/3}, \\ n_c = B_{sup} \exp[-D(T - T_c)] + n_0. \end{array} \right. \quad (69)$$

In Eq. (68) we call  $T_G$  the temperature on which the cluster of small size are gathering to form bigger cluster. This temperature marks the limit when one enters the critical region from below. In Eq. (68),  $\alpha$  is the half-width of the peak of  $n_c$  shown in Fig. 29.  $\rho_0$  is the resistivity at  $T = 0$  and  $\rho_\infty$  is that at  $T = \infty$ .

We summarize in Table 1 the different results obtained for the cases studied by MC simulations shown above. Other parameters  $A_{inf}$ ,  $B_{inf}$ ,  $C_{inf}$ ,  $A_{sup}$ ,  $B_{sup}$  and  $C_{sup}$  are fitting parameters which are not of physical importance and therefore not given here for the sake of clarity. Using the numerical values of Table 1 and the average cluster size and cluster number shown in Fig. 28 and Fig. 29, we plot Eqs. (68) and (69) by continuous lines in Figs. 21-26 to compare with MC simulations shown in these figures. We emphasize that our theory provides a good "fit" for simulation results.

Based on those results, we can extract the resistivity  $\rho_I$  corresponding only to the addition of impurities.  $\rho_I$  is defined as

$$\rho_I = \rho_m - \rho_{standard}, \quad (70)$$

where  $\rho_{standard}$  is the resistivity without impurities (see the first line of Table 1). We compare now the resistivity  $\rho_I$  with experiments realized by

Table 1. Various numerical values obtained by MC simulations which are used to plot Eqs. (68) and (69).

<i>Impurity</i>		$T_c$	$T_G$	$\nu_{inf}$	$\nu_{sup}$	$\alpha$
0%	S=1	9.58	7.4443 +/- 0.066	-0.9254 +/- 0.015	-0.2267 +/- 0.006	1.51875 +/- 0.07
1%	$\sigma=2$	9.68	7.5006 +/- 0.054	-0.9253 +/- 0.017	-0.1449 +/- 0.006	1.62908 +/- 0.06
2%	$\sigma=2$	9.63	7.7103 +/- 0.049	-0.9856 +/- 0.016	-0.1135 +/- 0.004	1.64786 +/- 0.05
5%	$\sigma=2$	10.2	7.9658 +/- 0.094	-1.1069 +/- 0.016	-0.0747 +/- 0.002	2.13618 +/- 0.10
1%	$\sigma=0$	9.47	7.2866 +/- 0.062	-0.9028 +/- 0.013	-0.2106 +/- 0.006	1.51766 +/- 0.06
5%	$\sigma=0$	9.10	7.0105 +/- 0.054	-0.9381 +/- 0.015	-0.1607 +/- 0.006	1.47261 +/- 0.05

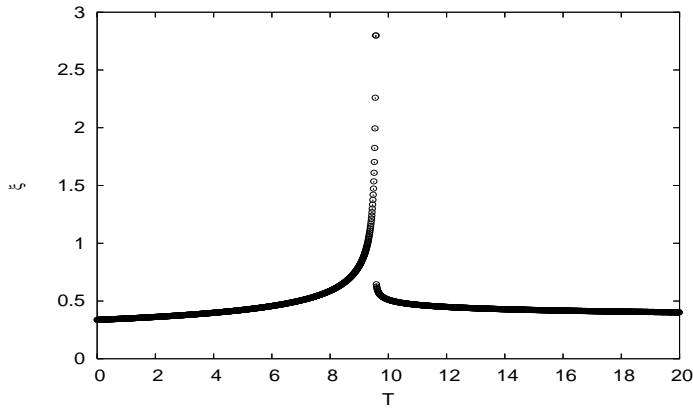


Fig. 28. Mean size  $\xi$  of magnetic clusters versus temperature  $T$  for both above and below  $T_c$ .

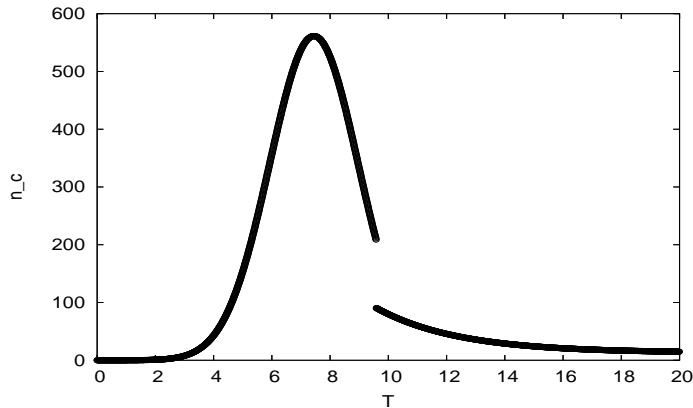


Fig. 29. Number of average cluster size  $n_c$  for both above and below  $T_c$ .

Schwerer and Cuddy.<sup>3</sup> It is important to note that the change of behavior can be explained if we use the correct value for  $\nu$ ,  $T_c$ ,  $T_G$ , etc. Figure 30 shows  $\rho_I$  with magnetic impurities corresponding to the Ni-Fe system, while Fig. 31 shows  $\rho_I$  in the case of non-magnetic impurities corresponding to the Ni-Cr case.

We see that the form of  $\rho_I$  of the alloys Ni-Fe(1%) and Ni-Fe(0.5%) experimentally observed<sup>3</sup> can be compared to the curves of 1% and 2% of magnetic impurities shown in Fig. 30. For Ni-Cr(1%) and Ni-Cr(2%), experimental curves are in agreement with our results of non-magnetic impurities

shown in Fig. 31.

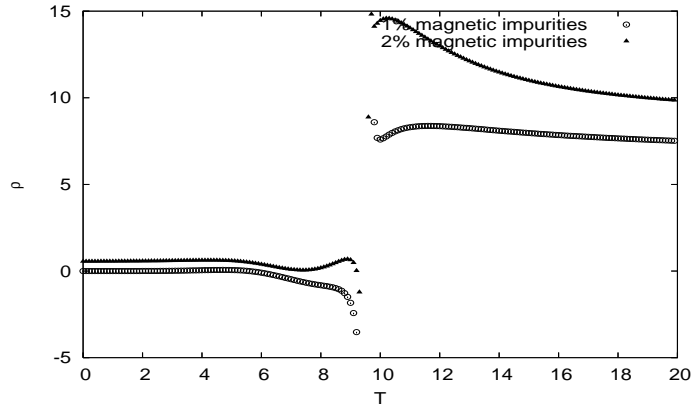


Fig. 30. Resistivity  $\rho_I$  in arbitrary unit versus temperature  $T$ . Void circles and black triangles indicate data for 1% and 2% magnetic impurities, respectively.

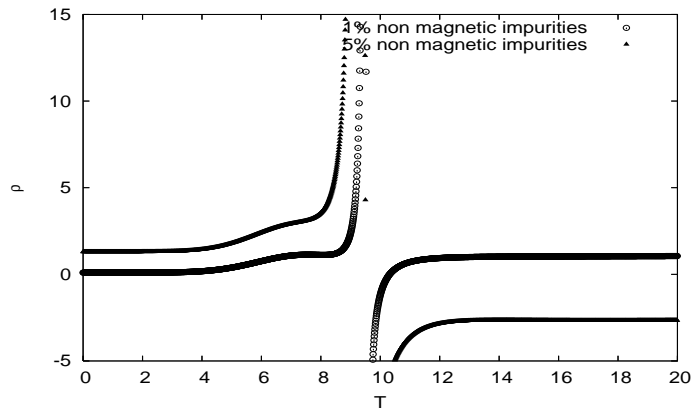


Fig. 31. Resistivity  $\rho_I$  in arbitrary unit versus temperature  $T$ . Void circles and black triangles indicate data for 1% and 5% non magnetic impurities, respectively.

Finally, to close this section, let us show theoretically from the equations obtained above, the effects of the density of itinerant spins on the resistivity. Figure 32 shows that, as the density  $n_0$  is increased, the peak of  $\rho$  diminishes. Our theory is thus in agreement with our MC results shown in section 5.5. It is noted that this behavior is very similar with that obtained

by Kataoka.<sup>16</sup> Let us emphasize that in the case of a weak density, one can keep the lattice spins unchanged upon interaction with itinerant spins. In the case of strong density, we expect that a number of lattice spins, when surrounded by a large number of itinerant spins, should flip to accommodate themselves with their moving neighbors. So the lattice ordering should be affected. As a consequence, critical fluctuations of lattice spins are more or less suppressed, so is the peak's height, just like in the case of an applied magnetic field. Kataoka<sup>16</sup> has found this in his calculation by taking into account the spin flipping: the resistivity's peak disappears then at the transition. We have also done this with MC simulation shown in section 5.5.

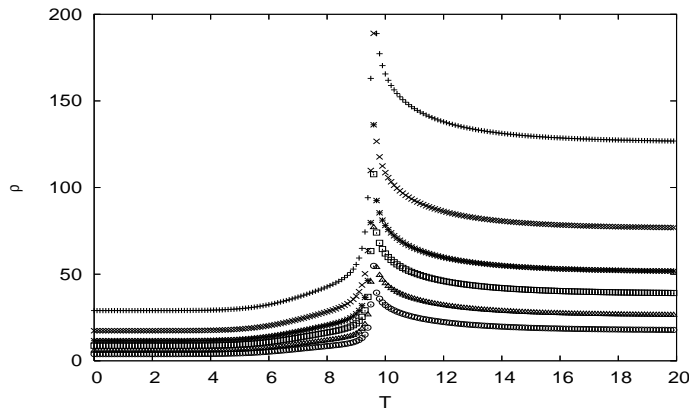


Fig. 32. Resistivity  $\rho$  in arbitrary unit versus temperature  $T$  for different densities of itinerant spins. Curves from top to bottom are for  $n_0 = 0.2, 0.33, 0.5, 0.7, 1$  and  $1.5$ .

## 7. Conclusion

We have reviewed in this chapter important works leading to the understanding of the resistivity behavior in magnetic systems. We have used a Monte Carlo method to study this problem which has not been used so far. We have shown results of MC simulations on the transport of itinerant spins interacting with localized lattice spins in a ferromagnetic FCC thin film. Various interactions have been taken into account. We found that the spin current is strongly dependent on the lattice spin ordering: at low  $T$  itinerant spins whose direction is parallel to the lattice spins yield a strong current, namely a small resistivity. At the ferromagnetic transition, the re-

sistivity undergoes a huge peak. At higher temperatures, the lattice spins are disordered, the resistivity is still large but it decreases with increasing  $T$ . From the discussion given in subsection 5.6, we conclude that the resistivity  $\rho$  of the model studied here behaves as the magnetic susceptibility with a peak at  $T_c$ .  $d\rho/dT$ , differential resistivity is thus negative for  $T > T_c$ . The peak of the resistivity obtained here is in agreement with experiments on magnetic semiconductors (Ga,Mn)As for example.<sup>6</sup> Of course, to compare the peak's shape experimentally obtained for each material, we need to refine our model parameters for each of them. But here, we were just looking for generic effects to show physical mechanisms lying behind the temperature dependence of the spin resistivity. In this spirit, we note that early theories have related the origin of the peak to the spin-spin correlation, while our interpretation here is based on the existence of defect clusters formed in the critical region. This interpretation has been verified by calculating the number and the size of clusters as a function of  $T$  by the use of Hoshen-Kopelman's algorithm. We have formulated a theory based on the Boltzmann's equation. We solved this equation using numerical data obtained for the number and the size of average cluster at each  $T$ . The results on the resistivity are in a good agreement with MC results.

The clear physical picture we provide in this work for the understanding of the behavior of the resistivity in a ferromagnetic film will help to understand properties of resistivity in more complicated systems such as antiferromagnets, non-Ising spin systems, frustrated spin systems and disordered media.

## References

1. P.-G. de Gennes and J. Friedel, *J. Phys. Chem Solids* **4**, 71 (1958).
2. A. Fert and I. A. Campbell, *Phys. Rev. Lett.* **21**, 1190 (1968); I. A. Campbell, *Phys. Rev. Lett.* **24**, 269 (1970).
3. F. C. Schwerer and L. J. Cuddy, *Phys. Rev.* **2**, 1575 (1970).
4. Alla E. Petrova, E. D. Bauer, Vladimir Krasnorussky, and Sergei M. Stishov, *Phys. Rev. B* **74**, 092401 (2006).
5. S. M. Stishov, A.E. Petrova, S. Khasanov, G. Kh. Panova, A.A.Shikov, J. C. Lashley, D. Wu, and T. A. Lograsso, *Phys. Rev. B* **76**, 052405 (2007).
6. F. Matsukura, H. Ohno, A. Shen and Y. Sugawara, *Phys. Rev. B* **57**, R2037 (1998).
7. M. N. Baibich, J. M. Broto, A. Fert, F. Nguyen Van Dau, F. Petroff, P. Etienne, G. Creuzet, A. Friederich and J. Chazelas, *Phys. Rev. Lett.* **61**, 2472 (1988).
8. P. Grunberg, R. Schreiber, Y. Pang, M. B. Brodsky and H. Sowers, *Phys.*

- Rev. Lett. **57**, 2442 (1986); G. Binash, P. Grunberg, F. Saurenbach and W. Zinn, Phys. Rev. B **39**, 4828 (1989).
9. A. Barthélémy et al, J. Mag. Mag. Mater. **242-245**, 68 (2002).
  10. See review by E. Y. Tsymlal and D. G. Pettifor, *Solid State Physics* (Academic Press, San Diego), Vol. 56, pp. 113-237 (2001).
  11. See review on Semiconductor Spintronics by T. Dietl, in Lectures Notes, vol. 712, Springer (Berlin), pp. 1-46 (2007).
  12. See review on Oxide Spintronics by Manuel Bibes and Agns Barthélémy, in a Special Issue of IEEE Transactions on Electron Devices on Spintronics, IEEE Trans. Electron. Devices **54**, 1003 (2007).
  13. P. P. Craig, W.I. Goldburg and al., Phys. Rev. Lett. **19**, 1334 (1967).
  14. M. E. Fisher and J.S. Langer, Phys. Rev. Lett. **20**, 665 (1968).
  15. S. Alexander, J. S. Helman and I. Balberg, Phys. Rev. B. **13**, 304 (1975).
  16. Mitsuo Kataoka, Phys. Rev. B **63**, 134435-1 (2001).
  17. K. Akabli, H. T. Diep and S. Reynal, J. Phys.: Condens. Matter **19**, 356204 (2007).
  18. K. Akabli and H. T. Diep, Phys. Rev. B **77**, 165433 (2008).
  19. R. Brucas and M. Hanson; J. Magn. Magn. Mater. **310**, 2521 (2007).
  20. J. Hoshen and R. Kopelman, Phys. Rev. B **14**, 3438 (1974).
  21. T. Kasuya, Prog. Theor. Phys. **16**, 58 (1956), No. 1.
  22. S. Legvold, F. H. Spedding, F. Barson and J. F. Elliott, Rev. Mod. Phys. **25**, 129 (1953).
  23. M. P. Kawatra, J. A. Mydosh, and J. I. Budnick, Phys. Rev. B **2**, 665 (1970).
  24. George Terence Meaden, *Electrical Resistance of Metals*, Plenum Press (1965).
  25. N. F. Mott, Proc. Phys. Soc. **47**, 571 (1935); N. F. Mott, Proc. Roy. Soc. **153**, 699 (1936); A. H. Wilson, Proc. Roy. Soc. **167**, 580 (1938).
  26. Diep-The-Hung, J. C. S. Levy and O. Nagai, Phys. stat. sol. **93**, 351 (1979).
  27. H. T. Diep, Phys. Rev. B **40**, 4818 (1989).
  28. H. T. Diep, Phys. Rev. B **43**, 8509 (1991).
  29. M. E. Fisher and R.J. Burford, Phys. Rev. **156**, 583 (1967).
  30. L. P. Kadanoff, Wolfgang Gotze and al. Reviews of Modern Physics Vol. **39**, No. 2, p. 395 (1967).
  31. C. Haas, Phys. Rev. **168**, 531 (1968).
  32. Y. Suezaki and H. Mori, Prog. Theor. Phys. **41**, 1177 (1969).
  33. T. Kasuya and A. Kondo, Solid State Commun. **14**, 249, 253 (1974).
  34. K. Binder and D. W. Heermann, *Monte Carlo Simulation in Statistical Physics*, Springer-Verlag, New York (1988).